Interactive comment on "Heterogeneous photochemistry of imidazole-2-carboxaldehyde: HO$_2$ radical formation and aerosol growth" by L. González Palacios et al.

We thank both of the reviewers for their helpful comments and suggestions. In the following we respond to all of the reviewer comments. The Reviewer Comment is first copied using regular text in black, followed by our response using italic font in blue. A copy of the text that we have changed in the manuscript is also added (in green) to facilitate a simultaneous consideration of the reviewers' comments and our replies where appropriate.

Anonymous Referee #1

Received and published: 16 March 2016

This is a nice manuscript that should be of great interest to the atmospheric community. HO$_2$ production from aerosols has not been widely investigated; this work suggests that it should not be ignored. I recommend that this manuscript be published following some minor revisions and clarifications.

Major comments:

Is the reaction occurring only at the surface, or also in the bulk? Did PHO$_2$ depend at all on film thickness? If only the surface reaction matters, then bulk phase diffusion (and reactions) can be ignored. If production in the bulk is important, I would expect HO2 production to depend on film thickness. Did it?

Response: The reaction occurs both in the bulk and at the surface of the studied films, as HO$_2$ production was observed for both solid and liquid (viscous) films. In the latter case, an experiment performed at PSI by PCA where IC:CA ratio was kept constant shows the classical behavior of reaction governed by reaction and diffusion (see figure below). At low thicknesses, P$_{HO2}$ increases linearly with thickness, but saturates at higher thickness above 2-3 µm. Therefore, P$_{HO2}$ represents clearly HO$_2$ production throughout the top few µm. HO2 produced further below is likely lost by self-reaction in the bulk.
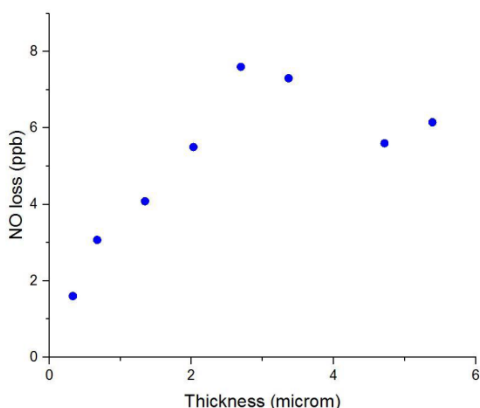
We have added this Figure in the SI text of the revised manuscript, and added some discussion in Section 3.1.

What is the expected extent of light attenuation throughout the film? If light is attenuated by the film, photolysis in CWFT experiments would occur primarily at the glass-film interface, and any HO_2 formed would have to diffuse to the surface before being released to the gas phase. Conversely, photolysis in the aerosol flow tube would occur primarily at the aerosol-air interface, and no diffusion would be required prior to HO_2 desorption to the gas phase. Could this explain the greater gas-phase HO_2 production in the aerosol flowtube compared to in the CWFT (either in addition to or in place of increased surface area of the aerosols)?

Response: The glass-film interface question can be answered by the response above. The films under study were about 3-4 μm; the above figure shows that these values are too thick for the glass-film interface to play a role in the HO_2 production observed.

For the light attenuation, we base our response on Figure S2. Our NO_2 actinometry studies show that there is not a significant decrease of photolysis to the gaseous NO_2 in the presence of a citric acid film (these studies were not performed in the presence of IC though). All photons need to penetrate the aqueous film before they can photolyze NO_2 in our setup, and if the film attenuated the light, there should be a significant decrease to the JNO_2 value when the film is present.

Notably, the IC is an optically thin absorber in our films. The optical density (O.D.) of IC in the film at 300 nm is 0.058, at 320 nm is 0.0095 and at 330 nm is 0.0019 (following Eq. O.D. = c × σ × l, where c is 0.300 M of IC in the film, the σ at 300 nm is 9.2 x 10^{-18} cm^2 molecule^{-1}, the σ at 320 nm is 1.5 x 10^{-18} cm^2 molecule^{-1}, and the σ at 330 nm is 3.0 x 10^{-19} cm^2 molecule^{-1} and l is 3.81 μm. Since the peak of the JIC spectrum is near 330 nm (Fig. S3), the effect of IC inside the film on the JIC is insignificant.

We believe that the higher production of HO_2 in aerosols (no diffusion needs to be accounted) is due to the potential higher reaction rate coefficient of limonene with the triplet state of IC compared to the reaction rate coefficient of citric acid. We assume this since in the AFT experiments, the concentration limonene that is exposed to the excited triplet state of IC is much lower than in the CWFT experiments.

In the Conclusion the authors state that HO_2 production is reduced at dry film surfaces due to increased viscosity (and therefore decreased IC and HO_2 mobility) within the film. Is it possible that the reactions occur at the surface and are enhanced by the presence of water? At what RH is a monolayer of water expected to exist at the film surface? Could ionized citric acid behave differently than molecular CA?

Response: Water seems to play a role when the H-donor is in the aqueous phase (compared to the aerosol studies where the H-donor is in the gas-phase, and low RH did not seem to have a significant effect on P_{HO2} as it did in the CWFT studies). Figure 5 further suggests a complex role of water. According to Zardini et al. (2008) pure citric acid solution does not effloresce; therefore, the film remained as a homogeneous aqueous solution under all RH conditions, and

thus the conclusion that the lower P_{HO2} is reduced due to lower diffusivity at low RH is well justified.

At the high citric acid activities of this study, acidity is very low, and citric acid predominantly is in its non-dissociated form. pH may have an effect on the absorbance of IC and thus probably on the P_{HO2}, but this was not investigated.

In the revised manuscript we have added the following in line 525 after P_{HO2}: "Zardini et al. (2008) demonstrates that pure citric acid does not efflorescence, this suggests, that the film remained as a homogenous aqueous solution under all RH conditions. This supports our conclusion that there is lower diffusivity at low RHs since the IC/CA reaction is favored by a certain amount of water molecules present, the range which has been previously stated."

Minor Comments:

Equation 1 uses 300 nm as a lower limit. Is this appropriate? Is light at that wavelength absorbed by the jacketed flow tube? Even a small change in the wavelength limits could change the calculated photon flux significantly.

Response: The limit at 300 nm is appropriate based on a limitation from the emission of the fluorescence lamps used (the emission below 300 nm is significantly low) and the material of the flow tube (DURAN glass, see http://www.duran-group.com/en/about-duran/duran-properties/optical-properties-of-duran.html). Since the peak of the JIC is near 330nm, and rapidly decreasing at shorter wavelengths (Fig. S3), changing the lower wavelength limit is not expected to change JIC more than the reported uncertainty in JIC.

Equation 1 also bases the absorption cross section of IC on that measured in aqueous solution. Is the absorbance of IC in a solid film expected to be the same as that in aqueous solution?

Response: Our films are not solid, but an aqueous solution of IC and CA. Nevertheless, matrix effects on the absorbance would deserve further investigation beyond the scope of the present study; we have allowed ample uncertainty on the calculated JIC to take into account such caveats.

There is only one data point at O2 levels greater than 55% shown in Figure 6. I would feel more comfortable with the stated conclusion that HO2 production decreases above 55% O2 with more measurements at higher O2 fractions.

Response: Lines 368-371, have been changed to: "We assume that at 55% O_2, the quenching of excited triplet states by O_2 has an effect on HO_2 production. This effect may decrease HO_2 production based on our results being qualitatively consistent with the observations of decreasing aerosol growth at high O_2 in the autophotocatalytic aerosol growth described in Aregahegn et al. (2013). However, the experimental focus of this study was based on atmospheric O_2 mixing ratios and thus we cannot conclude about the HO_2 production at high O_2 mixing ratios."

p. 4 lines 103-106: "... that in absence of other known radical sources confirm that HO2 production from aerosols can start photochemistry." I don't understand what this sentence means. Doesn't photochemistry form the HO2?

Response: The motivation for this sentence comes from the overarching role of gas phase radical sources in atmospheric chemistry. We have modified the sentence. It now reads: "Section 2.2 describe aerosol flow tube experiments that confirm the photochemical production of HO_2 radicals in the absence of other known gas-phase radical sources."

p.7 line 182-183: What do you mean by a "thin" film? Be a bit more quantitative.

Response: We have changed the sentence to: "…which was then dispersed into a thin ($3 - 4$ µm) and viscous film." We have also changed line 180 to: "The range of concentrations in the films was between $0.148 - 0.671$ M of IC and $5.29 - 6.68$ M of CA."

p. 11 line 303: "Each data point was measured from a freshly prepared coated film in the flow tube." What is meant by "each data point"? Figure 2 is a time series; presumably each data point was acquired during the same experiment (using the same film).

Response: We have changed the sentence to: "For irradiation, humidity and oxygen dependence experiments, each data point represents a separate experiment using a freshly prepared coated film in the flow tube."

p. 13 line 365: In describing Figure 6, the authors say that "A marginal decrease below 15% O2..." Marginal might not be the most appropriate term, since HO2 production decreases to zero in the absence of O2.

Response: We have removed 'marginal' here.

p. 18 line 508 -510: OH does not start Fenton reactions. Please reword.

Response: We have modified the sentence to read: "The unknown amount of HO_2 that remains in the condensed phase is a further source of OH in the same phase; this OH, in the presence of reduced metals, can trigger a cycle of Fenton reactions or other oxidizing pathways that can further age the aerosol."

Figure 4: What are the open circles in the plot?

Response: We have added a sentence in line 743: "The solid symbols represent the flux of HO_2 and the open circles represent the flux of HONO."

Anonymous Referee #2

Received and published: 20 March 2016

The work by González Palacios et al. provides indirect evidence for the formation of HO2 during photosensitized reactions of aerosols and thin surface films containing an imidazole and a H-atom donor (e.g., citric acid or limonene). This is a complicated system. The results are of high quality and appropriate methods and techniques were applied to the problem. I recommend publishing after the following points are addressed.

It was not clear how the data support that this reaction is autocatalytic? Are not autocatalytic processes characterized by a logistic product profile, whereas the NO2 vs time profile shown in Figure 2 show NO2 formed decreasing between 20 and 75 minutes. Is there any indication that this will level off at some significant steady state at later reaction times? On line 296-299 the authors state that the system only slowly evolves into a steady state; however how long does that take? If it does not reach steady-state, and the system ceases to convert NO into NO2 over time, then this is not an autocatalytic system.

Response: We have substituted the term 'autophotocatalytic' by 'photocatalytic'. We agree that our data do not allow for a firm conclusion about the autocatalytic nature of the mechanism. The initial autophotocatalytic statement applies to aerosol growth, not the CWFT films, and was based on previous studies (Aregahegn et al., 2013; Rossignol et al., 2014). We ran experiments in the CWFT overnight with a single film (> 10 hrs). Consistently the peak NO₂ production is observed shortly upon turning lamps ON; NO₂ reach sort of a plateau within the first hour, and in the overnight experiments NO₂ formation was always observed. While the 10hr integral HO₂ production rate is smaller than the added amount of IC, the 10hr integral photoexcitation rate of IC in the film is larger than the added amount of IC. Hence, the fact that NO2 formation is observed in the overnight experiments supports the photocatalytic claim. Notably, there is nothing in our data that would contradict the earlier conclusions in previous studies (Aregahegn et al., 2013; Rossignol et al., 2014).

The paragraph starting on Line 70 explains the motivation behind studying imidazole photochemistry. As stated by the authors, imidazole is thought to be generated from the reaction of glyoxal with ammonium and amines. The authors only discuss imidazole in SOA has been strictly in laboratory settings (see references cited), which may or may not be reflective of the real environment. I feel this section should include current views (for and against) on the importance of imidazole in atmospheric samples. The recent article by Teich et al. (ES&T 2016, 50, 1166) may be of help here. Such a discussion will help to better convey the atmospheric significance of this study.

Response: We have added discussion about field measurements of IC, including the results presented in Teich et al., 2016 in the revised manuscript.

The following text was added: "Field measurements of imidazoles are generally sparse, yet, recently Teich et al. (2016) identified five imidazoles (1-butylimidazole, 1-ethylimidazole, 2-ethylimidazole, IC and 4(5)-methylimidazole) in ambient aerosols in concentrations ranging

from 0.2 to 14 ng/m^3. IC, the molecule under study in this article, was measured in its hydrated form in ambient aerosols in three urban areas with signs of air pollution and biomass burning (Leipzig, Germany, Wuqing and Xianghe, China). The observed quantities of hydrated IC ranged from 0.9 to 3.2 ng/m. The authors claim that these values could be a lower limit due to high losses of IC during sample preparation indicated by low recovery from standard solutions. This suggests that IC and other imidazole derivatives are present in areas with high pollution and biomass burning. Field measurements in Cyprus during the CYPHEX campaign in 2014 detected IC and bis-imidazole in ambient aerosol samples (Jakob et al. 2015). The IC diurnal cycles showed the highest concentrations at night (0.02 – 0.115 ng/m^3), and lower concentrations during the day, suggesting that ambient concentrations of IC in aerosols are a balance between photochemical sources and sinks. While imidazoles seem to be widespread in polluted and remote areas, the atmospheric implications of IC, and possibly other photosensitizers related to brown carbon light absorption as radical sources in ambient aerosols deserve further study.*

Did the authors determine the concentration of nitrate present in their coatings during or following their reactions? When such high levels of NOx, it may be possible that some nitrate could be deposited to the surface. In such a case, photolysis of nitrate could release NO2 into the gas phase. Also, what was the pH of the films coating the glass walls? If citric acid was used this could have lowered the coating pH, in which case one must consider acid-base chemistry as well. This could impact organic photochemical reaction intermediates and also the yield of HO2, NO2 (via nitrate photolysis) and HONO generated in the system.

Response: We did not measure nitrate in either systems. However, this response follows Response #3 to Reviewer #1 (please see above). As stated above, the high CA concentrations in the studied films have a very low pH (not measured). According to studies from Laskin et al. (2014) in a citric acid-nitrate system HNO3 is in the gas-phase at low pH; this depletes nitrates by 45 – 55%, and lowers the chance of any photolyzed nitrate to contribute to the NO$_2$ observed.

We have added the following statement in the Conclusion section of the manuscript: "A systematic study of the effect of pH on the IC and CA absorption cross-sections, and the product yields from the IC photochemistry is desirable."

In the case of the aerosol flow reactor, citric acid was not used; Limonene was used instead, which would not acidify the particle. This represents a major difference between the CWFT and aerosol flowtube measurements that was not discussed. I would be interested in seeing if the authors think this difference could explain why NOx consumption in the aerosol system was so different than during the CWFT experiments.

Response: The higher NO$_x$ consumption in the AFT is probably the result of vigorous gas-phase secondary chemistry, possibly involving NO$_3$ radicals, and the longer reaction times in the AFT experiments; HNO$_3$ formation is further expected to result into significant acidification in the AFT experiments, but not in the CWFT experiments. The NOx consumption was not the focus of this study, and deserves further investigation.

line 40. The phrase, ". . .implications consist in a. . ." is awkwardly phrased. Perhaps revise to say rather: "Our results indicate a potentially relevant contribution. . ."

Response: We have adopted the reviewer suggestion.

line 58. Include "concentrations" after OH2

Response: Changed.

lines 83-84: Paragraph too long. I suggest inserting a paragraph break between these lines

Response: Changed.

lines 128-134: It appears that J-values for NO2 photolysis were calculated using clean flow tubes (i.e., in the absence of a coating). Therefore, one is assuming that the Jvalues for the clean tube are the same as those for a coated tube. Does the IC coating on the coated-wall flow tube attenuate the light enough to invalidate this assumption? If the IC coating does attenuate the light transmitted through the flowtube, how could this bias interpretation of the results?

Response: This is not correct. The actinometry was measured in a clean glass tube and in a citric acid coated flow tube – the IC absorption in the actinic window (see Fig. S3) is very small. See also our response to Reviewer #1.

line 253 (and other places where the term "H-donor" is used): The authors might want to clarify that the VOCs are H-atom donors, rather than proton donors as in the case of a Bronsted acid.

Response: We have clarified this. The following sentence was added to Section 1, line 91. The sentences after were made a new paragraph. "The citric acid and limonene are H-atom donors (referred to as H-donor from hereon), rather than proton donors as in the case of a Bronsted acid. In particular, the transfer of the H-atom leads to the formation of an alkyl-radical species. The H-atom transfer thus has the same effect as an H-atom abstraction reaction by Cl or OH radicals."

lines 314-318: It is not clear to me: Do the authors think that the NO to NO2 conversion by HO2 is occurring in the organic surface film or in the gas phase? How can they be sure?

Response: As stated above (see replies to reviewers 1, and new Figure added to the SI), the HO_2 formation occurs at the surface and in the bulk of the condensed phase. It is somewhat improbable that NO reacts with HO_2 in the condensed (due to low NO solubility); formation of NO_2 may occur at the interface and in the gas phase. The comparison between the AFT and CWFT data suggests that the NO to NO_2 conversion is happening in the gas-phase, since this is a very fast reaction, apparently observed with higher efficient in the system with the lower total surface area (AFT).

lines 319-323: The concentration of citric acid [CA] is in such excess relative to the imidazole. Could it not be assumed that [CA] is constant over the course of the experiments? In that case, why not just plot [HO2] vs [IC] instead of vs [IC]x[CA].

Response: CA is constant throughout all experiments, and thus it could be presented either way. We prefer to show the product of IC x CA due to CA representing an H-atom donor, and thus plays a crucial role in the mechanism.

lines 344-347: The authors discuss the role of coating viscosity on photochemistry. A recent article by Hinks et al. (PCCP, 2015, DOI: 10.1039/c5cp05226b) discusses this effect nicely and should be cited here.

Response: Thanks for pointing this out. The reference has been added. "Hinks et al. (2016) observed that the photodegradation rate of their studied secondary organic material increases with increased RH. This suggests that the motion of the molecules in a viscous film at a low RH is hindered and thus results in a lower photochemical reaction."

line 361: Cannot also H2O photophysically quench the triplet excited state? Is this important for this system?

Response: In laser photolysis experiments (not reported here), it was shown that oxygen may quench the triplet state of IC (without suppressing it even in oxygenated solutions – see figure below) and that the decay rate was first order in the H-donor. This is strongly suggestive of a minor role (if any) of the products of that reaction on the lifetime of the triplet state of IC
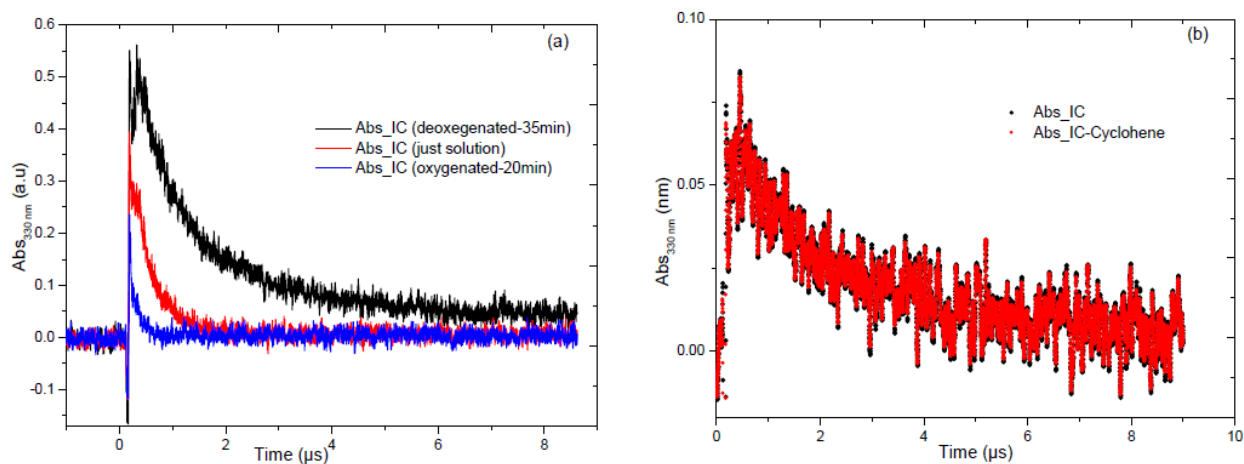
Figure 5-2 Triplet-triplet absorption of IC in water-acetonitrile (3:2);
(a) effect of degasing, (b) in the presence of cyclohexene.
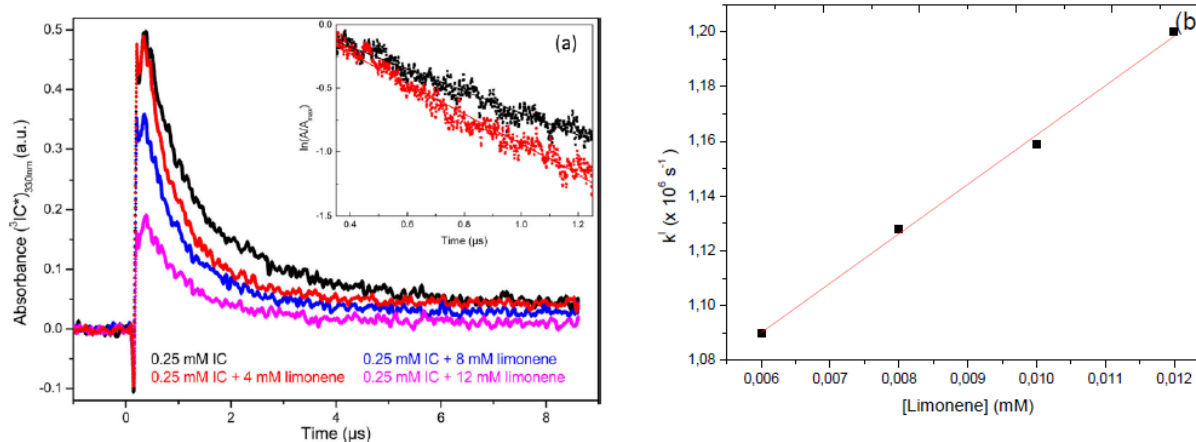
Figure 5-3 The change in the first order hate constant of IC for different limonene concentration; (a) transient absorption of excited triplet state of IC (0.25 m M). In the presence of (4 mM-Red), (8 mM – Blue) and (12 mM-pink) limonene; (b) first order hate constant as a function of limonene concentration.

lines 403-406: The authors mention that the photosensitizer 4-BBA behaves similar to IC. I would like to see this data included in the SI.

Response: The figures below have been added to the SI. The reader is reminded to see this Figure in the SI in Section 3.1.2.
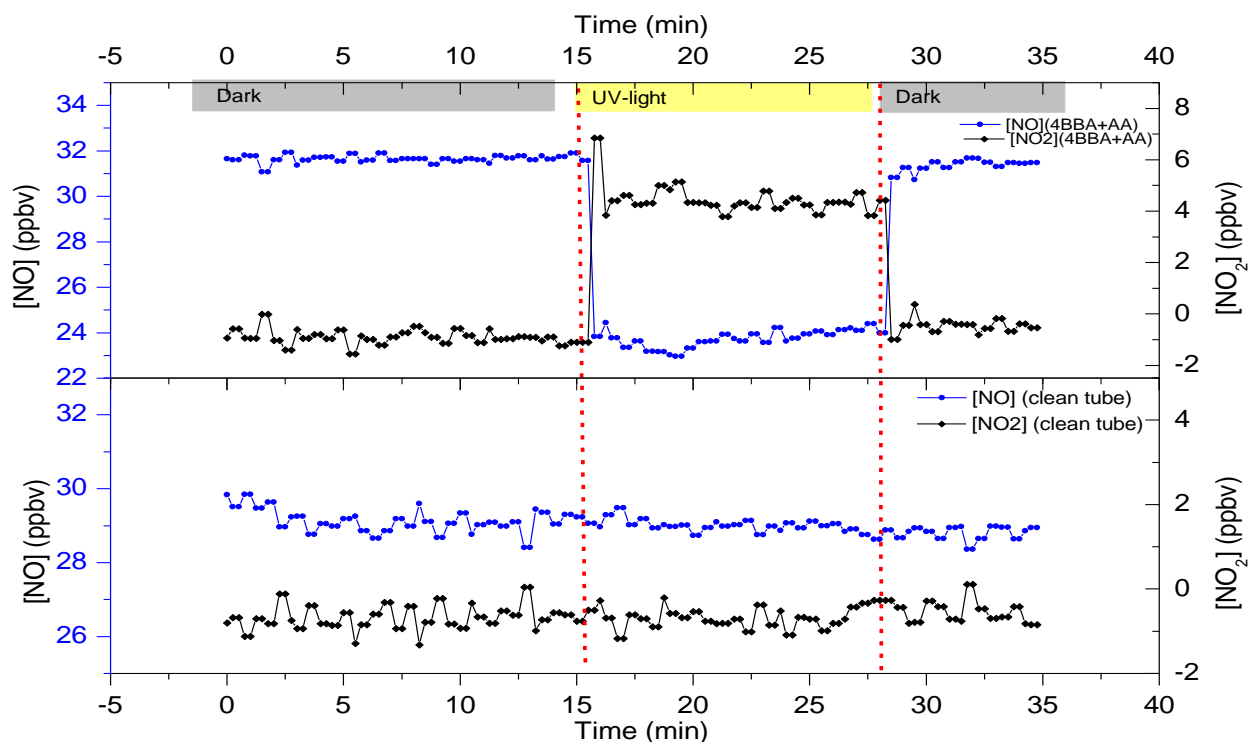
lines 426: With respect to ozone formation in the flowtube and aerosol systems, did the authors measure ozone and can they confirm that it was not observed in the system? Lifetimes of ozone were indicated for these experiments, do they account for heterogeneous loss as well?

Response: Ozone formation was measured to be ca. 20 ppbv in the AFT experiments in presence of NO. It was produced due to the significant extent of NO_2 photolysis during these experiments (operated with long residence times (ca. 20-50 min) and led to the secondary chemistry mentioned above (and in the manuscript). Secondary chemistry and O_3 formation were suppressed in the CWFT experiments (1 ppm NO, limited NO_2 photolysis over 2 sec residence time). We estimate the upper limit for the O_3 concentration < 0.5 ppby O_3. Attempts to measure O_3 during selected experiments showed it below the detection limit. This is the primary reason why we believe the CWFT provides more quantitative determinations of P_{HO2}.

Figure 8: Focusing on the "IM-C-OH(dot)" intermediate, should not the dot be centered on the carbon and not the alcohol H?

Response: This has been changed. Write as IM-C(dot)-OH.

Heterogeneous photochemistry of imidazole-2-carboxaldehyde: HO₂ radical formation and aerosol growth

Laura González Palacios[1,2], Pablo Corral Arroyo[3,4], Kifle Z. Aregahegn,[5,6,7], Sarah S. Steimer[3,54,87], Thorsten Bartels-Rausch[3], Barbara Nozière,[65], Markus Ammann[3,54], Christian George[65] and Rainer Volkamer[1,2]

[1]{University of Colorado, Department of Chemistry and Biochemistry, 215 UCB, Boulder, CO, 80309, USA}

[2]{University of Colorado, Cooperative Institute for Research in Environmental Sciences (CIRES), 216 UCB, Boulder, CO, 80309, USA}

[3]{Paul Scherrer Institute, Laboratory of Radio- and Environmental Chemistry, 5232 Villigen PSI, Switzerland}

[4] {University of Bern, Department of Chemistry and Biochemistry, 2012 Bern, Switzerland}

[5] {Swiss Federal Institute of Technology Zurich, Institute for Atmospheric and Climate Science, 8092 Zürich, Switzerland}

[65]{Université Lyon 1; Centre National de la Recherche Scientifique (CNRS), UMR5256, IRCELYON, Institut de recherches sur la catalyse et l'environnement de Lyon, F-69626 Villeurbanne, France}

[76]{now at: Chemistry Department, University of California, Irvine, California, 92697-202 }

[87]{now at: University of Cambridge, Department of chemistry, Cambridge CB2 1EW, UK}

Correspondence to: R. Volkamer (rainer.volkamer@colorado.edu).

Abstract

The multiphase chemistry of glyoxal is a source of secondary organic aerosol (SOA), including its light-absorbing product imidazole-2-carboxaldehyde (IC). IC is a photosensitizer that can contribute to additional aerosol ageing and growth when its excited triplet state oxidizes hydrocarbons (reactive uptake) via H-transfer chemistry. We have conducted a series of

1

27 photochemical coated-wall flow tube (CWFT) experiments using films of IC and citric acid (CA),

28 an organic proxy and H-donor in the condensed-phase. The formation rate of gas-phase HO_2

29 radicals (P_{HO2}) was measured indirectly by converting gas-phase NO into NO_2. We report on

30 experiments that relied on measurements of NO_2 formation, NO loss, and HONO formation. P_{HO2}

31 was found to be a linear function of (1) the [IC]×[CA] concentration product, and (2) the photon

32 actinic flux. Additionally, (3) a more complex function of relative humidity (25% < RH < 63%),

33 and of (4) the O_2/N_2 ratio (15% < O_2/N_2 < 56%) was observed, most likely indicating competing

34 effects of dilution, HO_2 mobility and losses in the film. The maximum P_{HO2} was observed at 25-

35 55% RH and at ambient O_2/N_2. The HO_2 radicals form in the condensed-phase when excited IC

36 triplet states are reduced by H-transfer from a donor, CA in our system, and subsequently react

37 with O_2 to re-generate IC, leading to a catalytic cycle. OH does not appear to be formed as a

38 primary product but is produced from the reaction of NO with HO_2 in the gas phase. Further, seed

39 aerosols containing IC and ammonium sulfate were exposed to gas-phase limonene and NO_x in

40 aerosol flow tube experiments, confirming significant P_{HO2} from aerosol surfaces. Our results

41 indicate a ~~Atmospheric implications consist in a~~ potentially relevant contribution of triplet state

42 photochemistry for gas-phase HO_2 production, aerosol growth and ageing in the atmosphere.

43

44 **1. Introduction**

45 The sources and sinks of radicals play an important role in the oxidative capacity of the

46 atmosphere. Radicals and other oxidants initiate the chemical degradation of various trace gases,

47 which is key in the troposphere (Jacob, 1999). The hydroxyl (OH) and peroxyl (HO_2) radicals

48 belong to the HO_x chemical family and are primarily generated by ultraviolet radiation

49 photochemical reactions (Calvert and Pitts, 1966), like the reaction of $O(^1D)$ (from O_3) with H_2O,

50 or photolysis of HONO, HCHO, H_2O_2, or acetone. Some secondary gas-phase sources are the

51 ozonolysis of alkenes or $O(^1D) + CH_4$ (Monks, 2005). The oxidation of VOCs by OH and other

52 oxidants in the presence of NO leads to perturbations in the HO_x, NO_x, and RO_x radical cycles that

53 affect O_3 and aerosol formation (Monks, 2005; Sheehy et al., 2010). The kinetics and

54 photochemical parameters of these reactions are relatively well-known in the gas-phase (Atkinson

55 et al., 2004; Sander et al., 2011). However, this does not apply to the sources and sinks for HO_x

56 in atmospheric droplets and on aerosol surfaces (Ervens et al., 2011). Uptake of OH from the gas-

57 phase, and H_2O_2 photolysis in the condensed phase are the primary known sources for HO_x in the

58 condensed-phase. HO_2 is highly soluble and the concentrations of OH, the most effective oxidant

59 in the condensed phase, depend on HO_2 radicals. Another source of HO_x radicals is from the

60 chemical reactions of reduced metal ions and H_2O_2, known as Fenton reactions (Fenton, 1894;

61 Deguillaume et al., 2005). Direct photolysis of H_2O_2, nitrite, nitrate (Zellner et al., 1990),

62 hydroperoxides (Zhao et al., 2013), and light absorbing secondary organic aerosol (SOA) (Badali

63 et al., 2015) are also sources of HO_x in the condensed-phase. Other studies have shown that the

64 photochemistry of iron (III) oxalate and carboxylate complexes, present in aqueous environments

65 (e.g. wastewater, clouds, fogs, particles), can initiate a radical chain reaction serving as an aqueous

66 source of HO_2 and Fe^{2+}. Fe^{2+} can then regenerate OH starting a new cycle of Fenton reactions

67 (Weller et al., 2013a, 2013b). The temperature dependent rate constants of OH in the aqueous

68 phase have been studied for a limited subset of organics (Ervens et al., 2003). However, there is

69 still a wide gap with respect to understanding the sources, sinks, kinetics and photochemical

70 reaction pathways of HO_x radicals in the condensed phase (George et al., 2015).

71 Our study investigates photosensitizers as an additional HO_x source that may be relevant to further

72 modify RO_x and NO_x reaction cycles in both the condensed- and gas-phases. It is motivated by

73 the formation of superoxide in terrestrial aqueous photochemistry (Draper and Crosby, 1983;

74 Faust, 1999; Schwarzenbach et al., 2002), by more recent observations that irradiated surfaces

75 containing titanium dioxide generate HO_x radicals in the gas-phase (Yi et al., 2012) and by the

76 generation of OH from metal oxides acting as photocatalysts in mineral dust (Dupart et al., 2012).

77 Past studies have demonstrated the reactivity of glyoxal towards ammonium ions and amines as a

78 source for light-absorbing brown carbon (Nozière et al., 2009; Galloway et al., 2009; Shapiro et

79 al., 2009; Kampf et al., 2012). One of these products is imidazole-2-carboxaldehyde (IC)

80 (Galloway et al., 2009), which absorbs light at UV wavelengths ($\lambda < 330$ nm) (Maxut et al., 2015).

81 Other imidazole-type compounds and light-absorbing products are formed in minor amounts but

82 can nonetheless impact optical and radiative properties of SOAs (Sareen et al., 2010; Trainic et

83 al., 2011). Photochemical reactions by these species are not typically accounted for in models yet,

84 but have a possible role for SOA formation and aerosol aging mechanisms (Sumner et al., 2014).

85 Photosensitizers are light absorbing compounds that absorb and convert the energy of photons into

86 chemical energy that can facilitate reactions, e.g., at surfaces or within aerosols (George et al.,

87 2015). For example, aerosol seeds containing humic acid or 4-(benzoyl)benzoic acid (4-BBA),

88 two other known photosensitizers, can induce the reactive uptake of VOCs when exposed to light,

89 leading to secondary organic aerosol (SOA) formation (Monge et al., 2012). Aregahegn et al.

90 (2013) and Rossignol et al. (2014) suggested a mechanism for autophotocatalyic aerosol growth,

91 where radicals are produced from the reaction of an H-donor hydrocarbon species, in this case

92 limonene, and the triplet state of IC. The condensed-phase citric acid and the gas-phase limonene

93 are H-atom donors (in this article we refer to them as H-donor), rather than proton donors as is the

94 case of a Brønsted acid. In particular, the transfer of the H-atom leads to the formation of an

95 alkyl-radical species. The H-atoms transfer thus has the same effect as an H-atom abstraction

96 reaction by Cl or OH radicals.

97 Field measurements on fog water samples confirmed that triplet excited states of organic

98 compounds upon irradiation can oxidize model samples such as syringol (a biomass burning

99 phenol) and methyl jasmonate (a green leaf volatile), accounting for $30 - 90\%$ of their loss (Kaur

100 et al., 2014). There are very few field measurements of imidazoles; a recent study by Teich et al.

101 2016 identified five imidazoles (1-butylimidazole, 1-ethylimidazole, 2-ethylimidazole, IC and

102 4(5)-methylimidazole in ambient aerosols in concentrations ranging from 0.2 to 14 ng/m^3. IC, the

103 molecule of interest in this study, was measured in its hydrated form in ambient aerosols in three

104 urban areas with signs of air pollution and biomass burning (Leipzig, Germany, Wuqing and

105 Xianghe, China). The observed quantities of hydrated IC ranged from 0.9 to 3.2 ng/m. The authors

106 claim that these values could be a lower limit due to high losses of IC during sample preparation

107 indicated by low recovery from standard solutions. This suggests that IC and other imidazole

108 derivatives are present in areas with high pollution and biomass burning. Field measurements in

109 Cyprus during the CYPHEX campaign in 2014 detected IC and bis-imidazole in ambient aerosol

110 samples (Jakob, Ronit, 2015). The IC diurnal cycles showed the highest concentrations at night

111 (0.02 – 0.115 ng/m3), and lower concentrations during the day, suggesting that ambient

112 concentrations of IC in aerosols are a balance between photochemical sources and sinks. While

113 imidazoles seem to be widespread in polluted and remote areas, the atmospheric implications of

114 IC, and possibly other photosensitizers related to brown carbon light absorption as radical sources

115 in ambient aerosols is another motivation to conduct this study.

116 The existence of such photocatalytic cycles could be of atmospheric significance. Canonica et al.

117 (1995) suggested indeed that the initial carbonyl, triggering the photochemical properties, is

118 regenerated via a reaction with oxygen producing HO$_2$. To our knowledge, the production of such

4

119 radical side products was not investigated under atmospheric conditions previously. We therefore
120 report here on the HO$_2$ radical production from IC in the condensed-phase.

121

2. Experimental Section

123 A series of flow tube experiments were conducted to investigate the formation of gas-phase HO$_2$
124 radicals from IC photochemistry using two different CWFT reactors (Sect. 2.1). Section 2.2
125 describes aerosol flow tube experiments ~~that in absence of other known radical sources~~ that
126 confirm th~~at~~e photochemical production of HO$_2$ radicals in the absence of other known gas-phase
127 radical sources in aerosols.~~production from aerosols can start photochemistry~~. All experiments
128 were performed at atmospheric pressure.

2.1. Coated-wall flow tube experiments

130 The CWFT experiments were designed to investigate the gas-phase production of HO$_2$ radicals
131 from a film containing IC and citric acid (CA) matrix as a function of UV light intensity, IC
132 concentration in the film, relative humidity (RH), and O$_2$ mixing ratio. Two similar experimental
133 setups were used as shown in Fig. 1. Some of the differences, not major, consist in the flow reactor
134 volume, surface area, flow rates, IC mass loading, NO mixing ratio, temperature inside the reactor
135 and the connected instrumentation.

136 **Setup 1.** Experiments were conducted in a photochemical flow-system equipped with a Duran
137 glass CWFT (0.40 cm inner radius, 45.2 and 40.0 cm length, inner surface = 113.6 and 100.4 cm^2,
138 S/V = 5.00 cm^{-1}), which was housed in a double jacketed cell coupled to a re-circulating water
139 bath to control the temperature at 298 K; The setup is shown in Fig. 1A. A thin film of IC+CA was
140 deposited inside the tubular glass flow tube. The experimental procedure for the preparation of
141 the films is described in Sect. 2.1.2. The system consisted of seven ultraviolet lamps (UV-A range,
142 Philips Cleo Effect 22 W: 300-420 nm, 41 cm, 2.6 cm o.d.) surrounding the flow tube in a circular
143 arrangement of 10 cm in diameter.

144 **Setup 2.** The second CWFT (CWFT 0.60 cm inner radius, 50 cm length, inner surface 188.5 cm^2,
145 S/V = 3.33 cm^{-1}) reactor had a glass jacket to allow water to circulate and maintain temperature
146 control inside the tube at 292 K. The coated-wall tubes were snuggly fit into the CWFT as inserts.
147 The CWFT was surrounded by the same seven fluorescent lamps as in Setup 1. The light passed

148   through different circulating water cooling jackets for both setups, thus providing a different light

149   path for each setup.

150   **Setup 1 and 2.** The actinic flux in the flow tube reactor, $F_{FT}(\lambda)$, was measured by actinometry of

151   NO_2 (see Supplement for description of J_{NO2} measurements), independently for both setups. The

152   flows of N_2, O_2, air and NO were set by mass flow controllers. The RH was set by a humidifier

153   placed after the admission of N_2 and O_2 gases but before the admission of NO or NO_2 (see Fig. 1),

154   in which the carrier gas bubbles through liquid water at a given temperature. The humidifier could

155   also be by-passed to set a RH of near zero. A typical measurement sequence is described in Sect.

156   2.1.2.

157   The J_{NO2} was measured for both Setup 1 and 2 using NO_2 actinometry. The J_{NO2} with seven lamps

158   was found to be 2×10^{-2} s^{-1} for Setup 1 and 1×10^{-2} s^{-1} for Setup 2 (see Fig. S12 for Setup 1, and

159   Supplemental Information text for both Setups). These values were compared to direct irradiance

160   measurements in the flow tube and thus normalized (see Sect. 3.1.1).

161

2.1.1. Flow tube instrumentation

163   The following gas-phase products exiting the flow tube were measured by three different

164   instruments: NO_2 by the University of Colorado Light Emitting Diode Cavity-Enhanced

165   Differential Optical Absorption Spectroscopy (LED-CE-DOAS) instrument (Thalman and

166   Volkamer, 2010), HONO by a LOng Path Absorption Photometer (LOPAP, QuMA Gmbh,

167   Heland, J., 2001; Kleffmann et al., 2002), and NO by a chemiluminescence analyzer (Ecophysics

168   CLD 77 AM, also used for NO_2 in Setup 2). HO_2 radicals were indirectly measured by detecting

169   NO_2 with the LED-CE-DOAS (Setup 1) and by the loss of NO with the chemiluminescence

170   detector (Setup 2). The latter was preceded by a molybdenum converter to transform HONO and

171   NO_2 to NO, and by an alkaline trap for HONO. Both, trap and converter, had a bypass to allow

172   sequential measurements and thereby obtaining the concentration of NO_2 and HONO separately.

173   HONO was measured by the LOPAP during some selected experiments (Kleffmann et al., 2002,

174   2006).

LED-CE-DOAS

The LED-CE-DOAS instrument (Thalman and Volkamer, 2010) detects NO_2 absorption at blue wavelengths. A high power blue LED light source (420–490 nm) is coupled to a confocal high finesse optical cavity consisting of two highly reflective mirrors (R = 0.999956) peaking at 460 nm that are placed about 87.5 cm apart (sample path length of 74 cm). The absorption path length depends on wavelength, and was about ~11 km near peak reflectivity here. A purge flow of dry nitrogen gas is added to keep the mirrors clean. The light exiting the cavity is projected onto a quartz optical fiber coupled to a Princeton Instruments Acton SP2156 Czerny-Turner imaging spectrometer with a PIXIS 400B CCD detector. The mirror reflectivity was calculated by flowing helium and nitrogen gas, exploiting the difference in the Rayleigh scattering cross sections of both gases as described in Thalman et al. (2014). The gas exiting the flow tube was directly injected into the CE-DOAS cavity, and spectra were recorded every 60 seconds, and stored on a computer. For analysis we use BBCEAS fitting at NO_2 concentrations exceeding few ppbv (Washenfelder et al., 2008) and DOAS least squares fitting methods at lower concentrations (Thalman et al., 2015). The mirror alignment was monitored online as part of every spectrum by observing the slant column density of oxygen collision complexes, O_2-O_2 (O_4) (Thalman and Volkamer, 2010, 2013). The following reference spectra were taken from the literature: NO_2 (Vandaele et al., 2002) and O_2-O_2 collision complexes (Thalman and Volkamer, 2013b). The detection limit for NO_2 was 50-100 pptv.

2.1.2. Experimental conditions

The IC+CA solutions were prepared by adding IC into a 1 M CA solution in 18 MΩ ultra-pure water to achieve IC to CA molecular ratios between 0.026 to 0.127 in the film. The bulk solutions for both sSetups were prepared by weighing out 384-400 mg of CA in 2 mL of water and adding 4-20 mg of IC to the solution. The solutions for both setups were freshly prepared for each experiment and the masses in the film were calculated at 50% RH from the CA hygroscopic growth factors reported by Zardini et al., 2008 for both setups (for Setup 1: 5-18 mg of IC and 44 mg of CA, for Setup 2: 1-5 mg of IC and 77 mg of CA). The range of concentrations in the films was between 0.148 – 0.671 M of IC and 5.29 – 6.68 M of CA.

The IC+CA solution coatings were produced by depositing 220-250 µL (Setup 1) and 400 µL (Setup 2) of the desired solution in a Duran glass tube, which was then dispersed into a thin and

205 viscous film _of 3 – 4 μm_ . The film was dried with a gentle N_2 stream humidified to a RH similar

206 to the experimental RH and room temperature. The film was rolled and turned upside down to

207 deposit a homogenous film throughout the entire inner surface of the flow tube. The homogeneity

208 of the film was confirmed by visual inspection. If a bright clear homogenous amorphous film from

209 the super-cooled solution was not observed, the film was discarded (e.g. observation of a turbid

210 and cracked crystallized appearance). The carrier gas flows consisted of premixed dry N_2 and O_2

211 (a ratio of 4.5/1 in Setup 1 and a ratio of 2 in Setup 2), and NO controlled by mass flow controllers.

212 The total flow rates were: 500 mL/min for Setup 1 and 1500 mL/min for Setup 2. In Setup 1, a

213 dilution flow of 1000 mL/min was added at the end of the flow tube for a total of 1500 mL/min

214 during experiments when HONO was measured along with NO_2. All experiments were conducted

215 at ambient pressure, leading to gas residence times of 2.1 – 2.4 s (depending on flow tube volume,

216 for both setups) under laminar flow conditions. The O_2 flow rate was varied between 0-110

217 mL/min to observe the dependence of O_2 while keeping the total flow rate constant. A ratio of

218 4.5:1 of N_2:O_2 was maintained if any of the other gas flows were changed (e.g. NO, and/or NO_2)

219 for Setup 1. For Setup 2, a ratio of 2:1 of N_2:O_2 was also maintained, except for the O_2

220 concentration dependence studies. The RH was kept constant at 50% RH during most experiments,

221 and varied between 10-60% RH to study humidity effects of the HO_2 radical production. The

222 concentration of NO was ~1 ppmv (Setup 1) and varied between 100 and 500 ppbv (Setup 2).

223 Scavenging of HO_2 was achieved by the following reaction:

$$NO + HO_2 \rightarrow NO_2 + OH \qquad\qquad (R1)$$
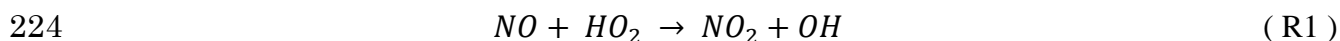
225 The lifetime of HO_2 is about 5 ms when 2.5×10^{13} molecules cm^{-3} of NO are present (Setup 1),

226 which assures efficient conversion of HO_2 molecules into NO_2 (k = 8.0×10^{-12} cm^3 molecule^{-1} s^{-1}

227 at 298 K, Sander et al., 2011). As shown in Fig. S2~~1~~, 500 ppbv NO, the concentration used in

228 Setup 2, was sufficient to efficiently convert HO_2 into NO_2, see Sect. 3.1.1. The lifetime of gas

229 phase HO_2 with respect to loss to the organic film is about 0.1 s, based on a similar formula shown

230 in Equation S3, where $\gamma = 10^{-3}$ (upper limit by Lakey et al., 2015). Note that in view of the

231 essentially diffusion controlled loss of HO_2 to the CWFT and tubing walls, the chosen scheme for

232 determining the production of HO_2 radicals from the films by fast scavenging with NO is superior

233 to a more selective detection method, e.g. LIF, which would require passing the HO_2 radicals into

234 a separate setup with substantial losses. For select_ed_~~ive~~ experiments, the films were exposed to

8

235 UV irradiation for over six hours which showed ~~a~~ only a minor change in the decrease of NO$_2$

236 concluding the stability of the reactivity of the films.

2.1.3. J_{IC} calculations

238 The absorption cross section of IC and the calculated photolysis rate are shown in Fig. S3. The

239 photolysis frequencies of IC were calculated using a similar procedure as described in

240 Schwarzenbach et al. (2002). The spectral irradiance in the flow tube system was interpolated to

241 the surface area of the flow tube to calculate the spectral photon flux density and the absorbed

242 photon flux:

$$F_a^{IC} = \int_{300}^{420} F \times [1 - 10^{-\sigma_{IC}(\lambda) \times b \times C_{IC}}]d\lambda, \qquad \text{where } F = \frac{F_{FT}(\lambda) \times SA}{N_a \times V_{film}}, \qquad (1)$$

244 Where F_a^{IC} is the mean absorbed photon flux in Ein L^{-1} s^{-1} nm^{-1} (1 Ein = 3.0 × 10^5 J per mole of

245 photons at 400 nm), F is the spectral flux density that reaches the film in the flow tube in moles L^{-1}

246 $^{-1}$ s^{-1} nm^{-1}, b is the optical path length taken as the thickness of the film and C_{IC} is the concentration

247 of IC in the film, and σ_{IC} is the IC absorption cross section. The absorption spectrum of IC in

248 water was based on the measurements by Kampf et al. (2012), and re-normalized to the peak value

249 of 10205 ± 2400 M^{-1} cm^{-1} at 284 nm (Maxut et al., 2015). V_{film} is the volume of the film calculated

250 from the deposited mass of CA and the hygroscopic growth factors of CA (Zardini et al., 2008),

251 SA is the surface area of the flow tube of the film, taken as the geometric area of the inner surface

252 area of the flow tube in cm^2, N_a is Avogadro's number in molecules mole^{-1}. The IC photoexcitation

253 rate J_{IC} was about 1.0 × 10^{-3} s^{-1} (upper limit).

254 We have also attempted to calculate an effective quantum yield for the formation of gas-phase

255 HO$_2$ radicals (ϕ_{HO2}):

$$P_{HO2} = \frac{[NO_2] \times flow}{N_a \times V_{film}} \qquad \qquad \phi_{HO2} = \frac{P_{HO2}}{F_a^{IC}} \qquad (2)$$

257 Where P_{HO2} is the HO$_2$ production rate in mol L^{-1} s^{-1}, F_a^{IC} is the calculated mean absorbed photon

258 flux by IC (Eq. 1), $[NO_2]$ is the gas-phase concentration of NO$_2$ in molecules cm^{-3} assuming a 1:1

259 ratio to HO$_2$ conversion, $flow$ is the volumetric gas flow at the temperature in the CWTF and

260 atmospheric pressure in cm^3 s^{-1}, and V_{film} is in L.

2.2. Aerosol flow-reactor experiments

A detailed description of the aerosol flow tube (AFT) is reported elsewhere (Monge et al., 2012; Aregahegn et al., 2013), therefore, only some principles are recalled below. The SOA experiments were conducted in a horizontal, cylindrical, Pyrex, aerosol flow reactor (13 cm i. d., 152 cm length) surrounded by seven UV lamps (Philips CLEO, 80W) with a continuous emission spectrum ranging from 300-420 nm (total irradiance of 3.31×10^{16} photons cm^{-2} s^{-1}). The flow reactor consisted of Teflon stoppers and different flow controllers that maintained the gas/aerosol/UV irradiation contact time between 20-50 minutes. This flow reactor also consisted of an outer jacket that controlled the temperature at 293 ± 2 K by water circulation using a thermostat (Model Huber CC 405).

Seed aerosols (50 nm) were produced by nebulizing a solution (at pH 6) containing ammonium sulfate (AS, 0.95 mM) and IC (1.3 mM), size selected by a DMA, and exposed to gas-phase limonene (500 ppbv) in the aerosol flow reactor. The typical aerosol mass loading in the reactor was 2-3 µg cm^{-3}, corresponding to ~15000 particles cm^{-3} with a starting diameter of 50 nm. As shown by Aregahegn et al. (in 2013), limonene is an efficient H-donor VOC that forms SOA via reactive uptake to IC containing seed aerosol. Due to the excess of limonene, and low seed aerosol surface are the consumption of limonene was below the detection limit. The aerosol growth was measured by means of an Ultrafine Condensation Particle Counter (UCPC) and a Scanning Mobility Particle Sizer Spectrometer (SMPS; both TSI), and similarly to the CWFT experiment, a flow of gaseous NO (from a 1 ppmv cylinder, Linde) was added to the carrier gas, and its conversion to NO_2 monitored by chemiluminescence detector with a detection limit of 0.05 ppbv (ECO PHYSICS CLD 88). Due to the long residence time, the NO_2 concentration is affected by its photolysis in the AFT. As discussed below, P_{HO2} was calculated, in this case, from the growth of the particle diameter measured at the exit of the flow tube; the assumption is that growth was due to reactive uptake of limonene only, and that each limonene forms one HO_2 radical. At 30 ppbv NO, the HO_2 radical lifetime is around 2 sec.

2.2.1. Experimental conditions

The total flow rate in the aerosol flow reactor was between 400 – 1000 ml/min, ensuring laminar flow conditions. The RH was varied between 0 – 50%. The RH of particles in the flow reactor was controlled by saturating the carrier gas via a bubbler containing ultra-pure water (Milli Q, 18

10

291   Mohm). The RH in the flow reactor system was varied by changing the gas flow rates to the

292   bubbler and the temperature of the circulating water jacket of the bubbler. The RH was measured

293   with a humidity sensor (Meltec UFT 75-AT, Germany) at the exit of the flow reactor. The

294   concentrations for the flow tube experiments were the following: 30 ppbv of NO and 500 ppbv of

295   limonene.

296   **2.3. Chemicals**

297   The following chemicals were used without further purification for CWFT studies: IC (97%,

298   Sigma Aldrich), and CA (Sigma Aldrich). For Setup 1, the Duran glass tubes were soaked in a

299   deconex® cleaning solution overnight, the next day they were rinsed with 18 MΩ water (Milli Q

300   Element system). These flow tubes were etched with a 5% hydrofluoric acid solution after the

301   washing procedure and again rinsed with water before any experimental use. The Duran flow

302   tubes for Setup 2 were not initially etched with any acid but stored in a NaOH solution after

303   washing and lastly rinsed with water; Setup 2 later confirmed that the treatment of flow tube with

304   acids affects P_{HO2} by rinsing with HCl and etching with HF solutions.

305   For the aerosol flow-reactor experiments gas-phase limonene was generated from commercially

306   available limonene (Aldrich, 97%) by means of a permeation tube. The following chemicals were

307   used without further purification: IC (97%, Sigma Aldrich) and succinic acid (Sigma Aldrich,

308     $\geq$99.5%);4-benzoylbenzoic acid (4-BBA, Aldrich 99%) and adipic acid (AA, Aldrich, $\geq$99.5%)

309   were used to expand the CWFT studies to other photosensitizers.

310

311   **3. Results and Discussion**

312   **3.1. Coated-wall flow tube**

313   The following results represent the light dependent formation of HO_2 indirectly from

314   measurements of NO_2 production and NO loss, measured with setup 1 and 2, respectively. Figure

315   2 shows a time series of NO_2 measured with setup 1 as a function of UV-A light, which confirms

316   the light dependent radical production. This particular film had an IC/CA ratio of 0.026 (0.148M

317   IC and 5.77M CA in the film). An evident increase of NO_2 is observed upon UV irradiation,

318   directly reflecting the light mediated release of HO_2, as shown in reaction (R1). The NO_2 signal

319 decreases over time with all seven lamps was a common feature observed in all films; this could

320 be due to HO_2 sinks in the film increasing with time, thus, the system only slowly evolves into a

321 steady state. A small amount of NO_2 (0.5-1.5 ppbv) was observed during experiments that used

322 only CA in absence of IC; therefore, the data in Fig. 2 and all data reported below have been

323 corrected for this NO_2 background, measured routinely in between experiments. Figure 2 also

324 indicates a strong correlation with irradiance, which is further discussed in the context of Fig. 4.

325 For irradiation, humidity and oxygen dependence experiments, eEach data point was

326 measuredrepresents a separate experiment using from a freshly prepared coated film in the flow

327 tube. The uncertainty for experiments was based on the standard deviation of n, the number of

328 experiments. The total uncertainty was $\pm$ 6-27% (propagated error for normalization was $\pm$ 7–

329 29%) for the IC mass loading experiments in Setup 1 and up to a factor of two for the light

330 dependence experiments. The uncertainty in Setup 2 was 10-50%. As discussed earlier, the

331 lifetime of HO_2 in the system was about three orders of magnitude less than the residence time in

332 the flow tube, therefore suggesting that most, if not all, reacted with NO to produce the observed

333 NO_2 (R1). Theoretically, the system was clean of other oxidants such as O_3 (and thus NO_3). The

334 uptake of NO_2 in the film was very small to further produce any nitrate radicals, and the photolysis

335 of NO_2 in the experiments to produce O_3 was insignificant ($< 1\%$). The recombination of NO and

336 O_3 contributes a negligible ($<0.1\%$) NO_2 source under our experimental conditions. RO_2

337 generation from the reaction between CA and OH from HONO photolysis was also ruled out since

338 it is approximated to account for only 1% of the NO_2 production if we assume every OH from the

339 photolysis reacts with CA. To our knowledge, the direct photolysis of CA to produce any RO_2

340 radicals has not been observed. Therefore, we believe that HO_2 is the essential oxidant for NO

341 and refer to the measured NO_2 as HO_2 formation.

342 Figure 3 shows that the HO_2 production fluxes, in molecules cm^{-2} min^{-1}, increased with IC mass

343 loading. The CA concentration was kept constant, and results are shown as the product between

344 [IC] $\times$ [CA], since we expect that the production rate of HO_2 is proportional to the concentration

345 of IC, at constant illumination, and that of the potential H-donor, CA. For Setup 1, the HO_2 fluxes

346 were measured as NO_2 mixing ratios, and calculated using the following equation:

347
$$Fluxes_{HO_2} = \frac{[NO_2] \times flow}{SA} \qquad (3)$$

348   the description of these parameters have been previously explained (see Sect. 2.1.3). For Setup 2,

349   the HO_2 flux was calculated similarly, but only about half of the observed NO loss was considered

350   to account for the loss of NO via the reaction with OH (see reaction in Supplement R1), meaning

351   that for each HO_2 scavenged two NO molecules were lost. In Figure 3, the data from Setup 1 are

352   represented by the black squares and the data from Setup 2 are represented by the gray circles.

353   Setup 1 measurements were taken at about ~50% RH and at room temperature. Setup 2

354   measurements were taken at 45% RH and at 292 K. Temperature has an effect on the observed

355   gas-phase HO_2 release from the film and thus needs to be accounted for, which is not accounted

356   for in Fig. 3 but it is described in detail in Sect. 3.1.1.

357   Figure 4 shows that the HO_2 production exhibited a linear dependence on the actinic flux for

358   various [IC] × [CA] molar products. From Sect. 2.1.3, we estimated an experimental ϕ_{HO2} of

359   about 6×10^{-5}, reflecting other probable, unknown quenching processes in our system. Figure 4

360   also shows the formation of HONO from three different IC mass loadings. In all three cases the

361    $HONO:NO_2$ ratio is < 1, confirming HO_2 as a primary product and OH as a secondary product.

362   Figure 5 shows the dependence of HO_2 production observed via the loss of NO (Setup 2) on

363   relative humidity $(0 - 65\%)$. Water partial pressure is an important parameter in the atmosphere

364   and it seems to also have an important effect on the photochemical reactions studied here. At RH

365   below ~10%, and at high RH above ~55%, the yield of HO_2 radicals decreases. The maximum

366   HO_2 radical production is observed at moderate RH $(20 - 55\%)$. This is probably due to a

367   combination of factors. In particular, at low RH the film may become more viscous reducing

368   mobility, and thus the energy transfer within the film. This may decrease the HO_2 yield as shown

369   in Fig. 5. Hinks et al. (2016) observed that the movement of molecules in a viscous film at a low

370   RH is hindered and thus decreases the photochemical reaction rate of secondary organic material.

371   The reduced diffusivity of HO_2 may also increase the residence time in the film and facilitate the

372   self-reaction in the bulk phase: The diffusivity of H_2O in citric acid is in the range of $10^{-7} - 10^{-8}$

373   cm^2s^{-1} at 50% RH. If the HO_2 diffusivity is between a factor of 10 and 100 lower than that of H_2O

374   due to its larger size, 10^{-9} cm^2s^{-1}, the first order loss rate coefficient for diffusion out of the film,

375   D/δ^2, δ denoting the film thickness $(4 \times 10^{-4}$ cm), becomes about $k_D = 10^{-2}$ s^{-1}. From the observed

376   F_{HO2}, the steady state concentration is then about $F_{HO2}/ k_D /\delta = 4 \times 10^{16}$ $cm^{-3} = 10^{-7}$ M. The loss rate

377   coefficient due to HO_2 self-reaction in the condensed phase $(7.8 \times 10^5$ M^{-1} $s^{-1})$ at this concentration

378   would become nearly 0.1 s^{-1}, somewhat higher than that for diffusional loss. Of course these

13

379   estimates carry a high uncertainty, but indicate that at lower humidity diffusivity gets low enough

380   to effectively reduce the diffusional loss of HO_2 to the gas phase and favor its loss by self-reaction

381   in the condensed phase. The potential presence of condensed phase sinks, such as RO_2, formed

382   from secondary chemistry of oxidized citric acid may add to this uncertainty. Figure S4 shows

383   that bulk diffusion can be neglected since any HO_2 produced below the first couple of micrometers

384   at the top of the film are likely lost to self-reaction in the condensed phase. This supplementary

385   experiment studied the thickness dependence of the films keeping the IC:CA ratio constant. The

386   results show that P_{HO2} increases linearly with thickness up to ~2.5 um, however, after this thickness

387   the film saturates, showing that this must happen at our films that are between $3-4$ µm thick. At

388   high RH ($> 55\%$), the amount of water associated with CA dilutes the reactants, and quenching of

389   the excited IC triplet states gains in relative importance, consistent with findings in other studies

390   (Stemmler et al., 2006, 2007; Jammoul et al., 2008). The RH effect can decrease the HO_2

391   production by a factor of 3, compared to the plateau of maximum HO_2 production between 20 –

392   55% RH.

393   Figure 6 shows the dependence of the HO_2 production based on the observed NO loss on the O_2

394   mixing ratio (Setup 2). The HO_2 production varied by about 20% over the range of conditions

395   investigated. A ~~marginal~~ decrease below 15% O_2 appears to be significant compared to the

396   maximum HO_2 production at ~40% O_2, indicating that O_2 is needed for HO_2 formation. Sufficient

397   O_2 dissolves in the aqueous phase to produce HO_2 radicals efficiently at atmospheric O_2 mixing

398   ratios. We assume that at ~~Above~~ 55% O_2, the ~~HO_2 production decreased, which is probably due~~

399   ~~to~~ quenching of excited IC triplet states by O_2 has an effect on HO_2 production This effect may

400   decrease P_{HO2} based on o~~O~~ur results being ~~are~~ qualitatively consistent with the observations of

401   decreasing aerosol growth at high O_2 in the autophotocatalytic aerosol growth described in

402   Aregahegn et al. (2013). However, the experimental focus of this study was based on atmospheric

403   O_2 mixing rations and thus we cannot conclude about the HO_2 production at high O_2 mixing ratios.

404   In order to test the possibility for excited IC triplet states to react with NO_2 at the surface of the

405   film, experiments were conducted with NO_2. While we did observe that the uptake of NO_2 on

406   irradiated surfaces scaled with light intensity (see Fig. S54) the reactive uptake coefficient of NO_2

407   to produce HONO at the surface is rather small ($< 2.5 \times 10^{-7}$), corresponding to a k_w of 10^{-3} s^{-1} and

408   thus neither a significant loss of NO_2 nor a significant source of HONO. The primary fate of the

409   nitrogen-containing aromatic alkoxy IC radical under atmospheric conditions is reaction with O_2.

410   However, we have not tested alternative quenching reactions of the triplet state, or other pathways

411   of the reduced ketyl radical that do not result into formation of HONO.

3.1.1 Comparison of data sets

413   The experimental conditions probed differ in the actinic flux, NO concentration, temperature, and

414   acidity. Here, we use the dependencies established in Sect. 3.1 to compare results from both setups.

415   The data from Setup 2 were normalized to conditions of Setup 1. The difference in J_{NO2}

416   corresponds to multiplying results from Setup 2 with a factor of 2.0 ± 0.1. HO_2 was measured

417   indirectly by reacting it with NO, and Fig. S21 indicates the minimum NO concentration needed

418   to efficiently scavenge all gas-phase HO_2 is ~460 ppbv of NO, indicating efficient conversion for

419   Setup 1, and a conversion efficiency of ~0.6 for Setup 2. The data from Setup 2 were multiplied

420   by 1.66 ± 0.10 to normalize for the NO conversion efficiency (Fig. S21), and by an additional

421   factor 1.25 ± 0.10 to match temperatures. We observed some limited variability depending on

422   whether HF or HCl were used to clean the flow tube prior to experiments. A higher P_{HO2} was

423   observed when cleaning with HF (Setup 1) compared to storing in NaOH and either rinsing with

424   water or HCl (Setup 2); this is accounted by multiplying data from Setup 2 with a factor of $1.25 \pm$

425   0.30. Notably, the error of the correction for the cleaning procedure that is propagated here is larger

426   than the correction factor. The effect of the pretreatment of the flow tubes was not systematically

427   studied, and thus remains a primary uncertainty in the comparison. No further correction was

428   applied for slight differences in RH. The overall correction factor amounts to 5.2 ± 1.4, with the

429   error reflecting the propagated uncertainty. This explains most the difference in P_{HO2} between both

430   setups. The normalized results agree within a factor of 2, which is a reasonably good agreement.

3.1.2 Extension to other photosensitizers

432   A limited number of experiments were performed using the CWFT approach, using 4-BBA as a

433   photosensitizer, in presence of 790 ppbv of gaseous limonene (a possible H-donor) and NO. The

434   organic thin film contained an organic acid matrix made of 4-BBA with/without adipic acid (AA).

435   Also in this system a substantial conversion of NO into NO_2 was observed (see Fig. S6). That 4-

436   BBA behaves similar to the IC system demonstrates that the chemistry discussed above can occur

437   on different excited carbonyls. It is interesting to note that this photo-induced conversion, and HO_2

438   production, was observed to be sustained over long times i.e., more than 15 h probably due to the

439   catalytic nature of the underlying chemical cycles. However, a fraction of the IC did get consumed

440   by photolysis reactions that do not form the excited triplet state (observed during overnight

441   experiments). The HO_2 flux for the 4-BBA system was estimated to be 2.77 x 10^{10} molecules cm$^-$

442   ^{2} min^{-1} making the same assumption that each HO_2 molecule reacts with NO to generate an NO_2

443   molecule. The calculation is based on Eq. 3, where it depends on the concentration of NO_2 as well

444   as the surface area and residence time.

445   **3.2. Aerosol Flow Tube**

446   The aerosol flow tube experiments were conducted similarly to the study by Aregahegn et al.

447   (2013), i.e., who demonstrated that in the absence of NO and known gas phase oxidants, seed

448   particles containing IC can initiate SOA growth in presence of a gaseous H-donor (limonene).

449   Figure 7 shows the results from similar experiments when NO was added to the system. No

450   conversion of NO to NO_2 was observed prior to the injection of limonene into the flow tube. The

451   presence of a gaseous H-donor and light clearly initiated a series of photochemical processes,

452   leading to SOA growth and gaseous NO_2 production. However, the quantitative interpretation

453   of these experiments is not straightforward due to efficient radical cycling in the

454   VOC/NO$_x$/light photochemical system, and the lack of a blank experiment that did not contain

455   IC as part of the seed particles. Limitations arise from the much longer residence time, which

456   allows NO_2 to be significantly photolyzed. The J_{NO2} was estimated as ~6.75 x 10^{-3} s^{-1}, and

457   corresponds to a photolysis lifetime of 2.5 minutes, which is smaller than the actual residence

458   time in the flow tube (~40 mins). Secondary chemistry can lead, among others, to ozone

459   production (O$_3$ lifetime at 500 ppbv limonene is ~7 min), and secondary OH radical formation

460   from the ozonolysis of limonene. Notably, NO$_x$ is not consumed in Fig. 7. The overall effect

461   of this secondary chemistry is an increased SOA growth compared to an experiment without

462   added NO (Aregahegn et al., 2013). As a consequence, the NO_2 yield cannot be used directly

463   to assess P_{HO2} in presence of NO.

464   However, in the absence of NO these secondary processes can largely be avoided, and are

465   reduced at a level where they cannot be identified (Aregahegn et al., 2013). Under such

466   conditions, the particle growth rates presumably carry information about the photosensitizer

467   cycling and subsequent HO_2 production. If we assume one molecule of limonene reacts to

468   produce one HO_2, the volume change of aerosols is proportional to the overall number of HO_2

469   produced. For example, a growth of 15,000 particles cm^{-3} from diameter 51.4 nm to 68.5 nm in 40

16

470   mins (residence time) is equal to P_{HO2} of 1.67×10^{14} molecules cm^{-2} min^{-1}. This should be

471   interpreted as an upper limit for the actual P_{HO2}, because water uptake may also be

472   contributing to the volume growth. However, compared to the CWFT experiments the much

473   higher surface to volume ratio of nanoparticles is expected to enhance the chemical coupling

474   of a gas-phase H-donor and the excited IC triplet state at the aerosol surface. This is at least

475   in part deemed responsible for the two orders of magnitude higher P_{HO2} in the aerosol flow

476   tube compared to the CWFT experiments. Notably, even if ϕ_{HO2} in the aerosol flow tube was

477   two order of magnitude higher than in the CWFT, it is still significantly smaller than unity.

478   **Primary HO$_2$ formation from IC**

479   One of the main advantages of the CWFT is that it operates at much shorter residence time. From

480   Setup 1, we derive a P_{HO2} of 1.76×10^{12} molecules cm^{-2} min^{-1} for IC/CA = 0.1 and $J_{NO2} = 8 \times 10^{-3}$

481   ^{3} s^{-1}. This corresponds to 2.9×10^{4} molecules cm^{-3} s^{-1} once normalized by aerosol surface area

482    $(1.18 \times 10^{-6}$ cm^{2} cm$^{-3})$, and J_{NO2} in the aerosol flow tube. Such a primary radical flux is equivalent

483   to the OH radical production rate resulting from photolysis of ~1 pptv of HONO in the aerosol

484   flow tube. Conversely, a P_{HO2} of 1.67×10^{14} molecules cm^{-2} min^{-1} is equivalent to the OH radical

485   production rate from ~100 pptv HONO in the aerosol flow tube. We conclude that seed particles

486   containing IC contribute significantly (equivalent to 1-100 pptv HONO) to the primary HO$_x$ radical

487   production rate in the aerosol flow tube experiments in the presence of NO (Fig. 7). Primary HO$_2$

488   radicals formed from IC containing seed particles react rapidly with NO to form OH radicals under

489   the conditions shown in Figure 7. The H-donor species is further expected to form primary RO$_2$

490   radicals. These primary HO$_2$ and RO$_2$ radicals add directly to the conversion of NO into NO$_2$, and

491   indirectly by driving secondary NO-to-NO$_2$ conversion from the RO$_2$/HO$_2$ radical chain. The

492   aerosol flow tube experiments thus qualitatively confirm the results obtained from macroscopic

493   surfaces, and highlight the potentially important role of surface-to-volume ratio and gaseous H-

494   donors to enhance the relevance of H-donor photochemistry as sources for HO$_x$/RO$_x$ radicals and

495   SOA.

496   **3.3. Proposed mechanism**

497   A mechanism that can describe the results from the CWFT experiments is shown in Fig. 8. It

498   follows the mechanism first proposed by Canonica et al., in 1995. The primary product in our

499   system is the HO$_2$ radical, which forms from the reaction between a nitrogen-containing aromatic

17

500   alkoxy IC radical and a ground state oxygen molecule, recycling the IC molecule. The aromatic

501   alkoxy radicals form from the excited triplet state of IC via transfer of an H atom from an H-donor

502   (in our case likely to be CA, or the CA/H_2O matrix). While a fraction of the IC will get consumed

503   by photolysis reactions that do not form the excited triplet state (see Sect 3.1.2.), IC is also

504   continuously produced from multiphase reactions, e.g., of glyoxal (Yu et al., 2011; Kampf et al.,

505   2012; Maxut et al., 2015). Another conclusion is that OH is a secondary product. If OH was a first

506   generation product we would have expected HONO:NO_2 ratios larger than 1:1. A smaller ratio

507   was observed, as shown in Fig. 4, indicating that there was no direct evidence for primary

508   formation of OH radicals. Interestingly, the H-donor species becomes activated as a result of H-

509   abstraction, and can react further to produce organic peroxy radicals, as evidenced by the aerosol

510   flow tube results.

511

512   **4. Atmospheric relevance**

513   The atmospheric relevance of our findings consists of the possible effect of heterogeneous radical

514   sources to modify atmospheric HO_2 radical concentrations, and facilitate aerosol growth and

515   ageing by adding a radical source within aerosol particles. The production of ~~gas-phase~~ HO_2 from

516   IC photosensitized heterogeneous chemistry is a possible source of gas-phase HO_2 radicals in

517   ambient air. In order to estimate the possible relevance for HO_2 radical concentrations in urban air,

518   we assume P_{HO2} of 2×10^{12} molecules cm^{-2} min^{-1} (IC/CA = 0.1, Setup 1) as a lower limit, and 2

519   $\times 10^{14}$ molecules cm^{-2} min^{-1} (IC/AS = 0.1, aerosol flow tube) as an upper limit, and typical

520   conditions in Mexico City (i.e., $J_{NO2} = 8 \times 10^{-3}$ s^{-1} at noontime in Mexico City, aerosol surface

521   area = 15 cm^2 m^{-3}; Volkamer et al., 2007). The normalized P_{HO2} during noon time in Mexico City

522   ranges from 2×10^5 to 2×10^7 molecules cm^{-3} s^{-1}. This corresponds to a rate of new HO_2 radical

523   production of 4 to 400 pptv/hr HONO around solar noon in Mexico City (Li et al., 2010), where

524   other radical sources produce about 5.9×10^7 molecules cm^{-3} s^{-1} at solar noon (Volkamer et al.,

525   2010). The upper range value suggests that aerosol surfaces can be a significant source of gas-

526   phase HO_x in places like Mexico City. However, the IC molar ratios used here are likely an upper

527   limit compared to ambient aerosols, yet, in principle other brown carbon molecules (i.e. HULIS

528   and/or other imidazole derivatives) may form additional gas-phase HO_2. The heterogeneous HO_2

529   radical source could further be relatively more important in unpolluted regions under biogenic

18

530   influences, where gas-phase radical production rates are lower. A more comprehensive

531   characterization of the heterogeneous HO_2 source effect on gas-phase HO_2 radical concentrations

532   hence deserves further investigation.

533   OH radical uptake from the gas-phase is a primary OH source in aerosols (Ervens and Volkamer,

534   2010). Assuming a gas-phase OH concentration of 10^6 molecules cm^{-3}, 15 cm^2 m^{-3} aerosol surface

535   area, and γ_{OH} of unity, the rate of OH uptake is approximately 2.3×10^5 molecules cm^{-3} s^{-1}. The

536   above estimated P_{HO2} is a result from H-transfer to form organic peroxy radicals which is

537   comparable to the rate of OH uptake. The two similar estimates of HO_x suggest that IC is a

538   significant source of radicals in the condensed phase of particles. This is a lower limit due to the

539   unknown radical losses of HO_x to the condensed phase, which hold potential to leverage the HOx

540   source by up to a factor 10,000 if limited by the IC excitation rate. The unknown amount of HO_2

541   that remains in the condensed-phase is a further source of OH in the ~~condensed~~ same phase; this

542   OH, in the presence of reduced metals, ~~that~~ can trigger a cycle of ~~start~~ Fenton reactions ~~(if iron is~~

543   ~~present)~~ or other oxidizing pathways that can further age the aerosol.

544   These results show that IC, and other aromatic carbonyl photosensitizers, are likely a relevant

545   radical source in aerosol particles. Photo-induced radical generation in condensed phases is

546   currently not represented in atmospheric models that describe aerosol ageing, and warrant further

547   study.

548

5. Conclusion

550   Three different experimental setups consistently show that HO_2 radicals are produced from the

551   photochemistry of IC in a CA+H_2O matrix and in seed aerosols containing ammonium sulfate (in

552   presence of a gas-phase H-donor, limonene). The linear correlations of P_{HO2} (with [IC]/[CA] and

553   irradiation) yielded maximum P_{HO2} under atmospherically relevant irradiation, O_2 and RH, but

554   also revealed a complex role of film viscosity, and possibly acidity effects (a systematic study of

555   the effect of pH on the IC and CA absorption cross-sections and the product yields from the IC

556   photochemistry is desirable). If the H-donor species is in the condensed phase, significant amounts

557   of HO_2 reach the gas-phase only for moderately high RH (~25 – 55% RH) that facilitates H-

558   transfer, and allows molecules (IC, HO_2) to move freely towards the surface of the film. When

559   the film was too dry this mobility is inhibited due to enhanced viscosity and significantly decreases

560 the P_{HO2}. At RH and O_2 higher than 55%, we observe a decrease in P_{HO2} probably due to dilution

561 by water and competing quenching reactions in the film. We know from Zardini et al. (2008) that

562 pure citric acid does not efflorescence and thus the film remains homogenous in its aqueous phase

563 under all RH conditions. This supports our conclusion that the P_{HO2} is RH dependent since it is

564 partially controlled by the diffusivity in the film. On the contrary, if the H-donor species is in the

565 gas-phase, significant HO_2 production is also observed under dry conditions. The primary fate of

566 the IC•-OH radical at the surface is reaction with O_2 to form HO_2. NO_2 reactions do not appear to

567 form HONO at the surface. Our results suggest that the radical source from photosensitizers such

568 as IC can help jump-start photochemistry of VOCs. The effect on the gas-phase HO_2 radical

569 concentration increases for higher surface to volume ratio of aerosols, and in the presence of gas-

570 phase H-donors. The autophotocatalytic growth of aerosols containing photosensitizers via H-

571 donor chemistry is a SOA source also in the presence of NO, and adds oxidative capacity inside

572 aerosol particles. Further research on other types of H-donors and photosensitizers is necessary to

573 compare different P_{HO2} and rates of aerosol growth from reactive uptake of VOC that could

574 potentially have a significant atmospheric relevance for SOA formation and heterogeneous aerosol

575 ageing.

Author contributions

577 M.A. and R.V. designed the experiments at PSI; C.G. and B.N. those at IRCELYON. L.G.P.,

578 P.C.A., and K.Z.A. conducted the measurements, analyzed data, and contributed equally to this

579 work. S.S.S., T.B.R. helped during the experiments, and all co-authors contributed to the data

580 interpretation. L.G.P. and R.V. prepared the manuscript with contributions from all co-authors.

581

References

Aregahegn, K. Z., Nozière, B. and George, C.: Organic aerosol formation photo-enhanced by the formation of secondary photosensitizers in aerosols, Faraday Discuss., 165(0), 123–134, doi:10.1039/C3FD00044C, 2013.

Atkinson, R., Baulch, D. L., Cox, R. A., Crowley, J. N., Hampson, R. F., Hynes, R. G., Jenkin, M. E., Rossi, M. J. and Troe, J.: Evaluated kinetic and photochemical data for atmospheric chemistry: Volume I - gas phase reactions of Ox, HOx, NOx and SOx species, Atmos Chem Phys, 4(6), 1461–1738, doi:10.5194/acp-4-1461-2004, 2004.

Badali, K. M., Zhou, S., Aljawhary, D., Antiñolo, M., Chen, W. J., Lok, A., Mungall, E., Wong, J. P. S., Zhao, R. and Abbatt, J. P. D.: Formation of hydroxyl radicals from photolysis of secondary organic aerosol material, Atmos Chem Phys, 15(14), 7831–7840, doi:10.5194/acp-15-7831-2015, 2015.

Calvert, J. G. and Pitts, J. N.: Photochemistry, Wiley, New York., 1966.

Canonica, S., Jans, U., Stemmler, K. and Hoigne, J.: Transformation Kinetics of Phenols in Water: Photosensitization by Dissolved Natural Organic Material and Aromatic Ketones, Environ. Sci. Technol., 29(7), 1822–1831, doi:10.1021/es00007a020, 1995.

Deguillaume, L., Leriche, M., Desboeufs, K., Mailhot, G., George, C. and Chaumerliac, N.: Transition metals in atmospheric liquid phases: sources, reactivity, and sensitive parameters, Chem. Rev., 105(9), 3388–3431, doi:10.1021/cr040649c, 2005.

Draper, W. M. and Crosby, D. G.: Photochemical generation of superoxide radical anion in water, J. Agric. Food Chem., 31(4), 734–737, doi:10.1021/jf00118a014, 1983.

Dupart, Y., King, S. M., Nekat, B., Nowak, A., Wiedensohler, A., Herrmann, H., David, G., Thomas, B., Miffre, A., Rairoux, P., D'Anna, B. and George, C.: Mineral dust photochemistry induces nucleation events in the presence of SO2, Proc. Natl. Acad. Sci. U. S. A., 109(51), 20842–20847, doi:10.1073/pnas.1212297109, 2012.

Ervens, B., Gligorovski, S. and Herrmann, H.: Temperature-dependent rate constants for hydroxyl radical reactions with organic compounds in aqueous solutions, Phys. Chem. Chem. Phys., 5(9), 1811–1824, doi:10.1039/b300072a, 2003.

Ervens, B., Turpin, B. J. and Weber, R. J.: Secondary organic aerosol formation in cloud droplets and aqueous particles (aqSOA): a review of laboratory, field and model studies, Atmos Chem Phys, 11(21), 11069–11102, doi:10.5194/acp-11-11069-2011, 2011.

Faust, B. C.: Aquatic Photochemical Reactions in Atmospheric, Surface, and Marine Waters: Influences on Oxidant Formation and Pollutant Degradation, in Environmental Photochemistry, edited by D. P. Boule, pp. 101–122, Springer Berlin Heidelberg. [online] Available from: http://link.springer.com/chapter/10.1007/978-3-540-69044-3_4 (Accessed 7 December 2015), 1999.

623 Fenton, H. J. H.: LXXIII.?Oxidation of tartaric acid in presence of iron, J. Chem. Soc. Trans., 65,
624 899, doi:10.1039/ct8946500899, 1894.

625 Galloway, M. M., Chhabra, P. S., Chan, A. W. H., Surratt, J. D., Flagan, R. C., Seinfeld, J. H.
626 and Keutsch, F. N.: Glyoxal uptake on ammonium sulphate seed aerosol: reaction products and
627 reversibility of uptake under dark and irradiated conditions, Atmos Chem Phys, 9(10), 3331–
628 3345, doi:10.5194/acp-9-3331-2009, 2009.

629 George, C., Strekowski, R. S., Kleffmann, J., Stemmler, K. and Ammann, M.: Photoenhanced
630 uptake of gaseous NO2 on solid organic compounds: a photochemical source of HONO?,
631 Faraday Discuss., 130, 195–210; discussion 241–264, 519–524, 2005.

632 George, C., Ammann, M., D'Anna, B., Donaldson, D. J. and Nizkorodov, S. A.: Heterogeneous
633 Photochemistry in the Atmosphere, Chem. Rev., doi:10.1021/cr500648z, 2015.

634 Heland, J., J. K.: A new instrument to measure gaseous nitrous acid (HONO) in the atmosphere.,
635 Environ. Sci. Amp Technol., 35(15), 3207–12, doi:10.1021/es000303t, 2001.

636 Hinks, M. L., Brady, M. V., Lignell, H., Song, M., Grayson, J. W., Bertram, A. K., Lin, P.,
637 Laskin, A., Laskin, J. and Nizkorodov, S. A.: Effect of viscosity on photodegradation rates in
638 complex secondary organic aerosol materials, Phys. Chem. Chem. Phys., 18(13), 8785–8793,
639 doi:10.1039/C5CP05226B, 2016.

640 Jacob, D.: Introduction to Atmospheric Chemistry, Princeton University Press, Princeton, N.J.,
641 1999.

642 Jakob, Ronit: Entwicklung von chiralen- sowie RP-HPLC- Methoden in Verbindung mit
643 hochaufloesender MS und deren Anwendung zur Analyse sekundaerer organischer Aerosole in
644 der Atmosphaere, Doktor der Naturwissenchaften, Johannes Gutenberg-Universitaet Mainz,
645 Mainz, Germany., 2015.

646 Jammoul, A., Gligorovski, S., George, C. and D'Anna, B.: Photosensitized Heterogeneous
647 Chemistry of Ozone on Organic Films, J. Phys. Chem. A, 112(6), 1268–1276,
648 doi:10.1021/jp074348t, 2008.

649 Kampf, C. J., Jakob, R. and Hoffmann, T.: Identification and characterization of aging products
650 in the glyoxal/ammonium sulfate system – implications for light-absorbing material in
651 atmospheric aerosols, Atmos Chem Phys, 12(14), 6323–6333, doi:10.5194/acp-12-6323-2012,
652 2012.

653 Kaur, R., Anastasio, C., Valsaraj, K. T., Vempati, H. S. and Vaitilingom, M.: Photoformation of
654 Triplet Excited States and Other Oxidants in Fog Waters and Their Impact on Fog Processing of
655 Organic Compounds, AGU Fall Meet. Abstr., 53, 07, 2014.

656 Kleffmann, J., Heland, J., Kurtenbach, R., Lörzer, J. C. and Wiesen, P.: A new instrument
657 (LOPAP) for the detection of nitrous acid (HONO), Environ. Sci. Pollut. Res., 9(4), 48–54,
658 2002.

22

659 Kleffmann, J., Wiesen, P. and Kern, C.: Intercomparison of the DOAS and LOPAP techniques
660 for the detection of nitrous acid, 2006.

661 Lakey, P. S. J., George, I. J., Whalley, L. K., Baeza-Romero, M. T. and Heard, D. E.:
662 Measurements of the HO2 Uptake Coefficients onto Single Component Organic Aerosols,
663 Environ. Sci. Technol., 49(8), 4878–4885, doi:10.1021/acs.est.5b00948, 2015.

664 Li, G., Lei, W., Zavala, M., Volkamer, R., Dusanter, S., Stevens, P. and Molina, L. T.: Impacts
665 of HONO sources on the photochemistry in Mexico City during the MCMA-2006/MILAGO
666 Campaign, Atmos Chem Phys, 10(14), 6551–6567, doi:10.5194/acp-10-6551-2010, 2010.

667 Maxut, A., Noziere, B., Fenet, B. and Mechakra, H.: Formation Mechanism and yield of small
668 Imidazoles from Reactions of Glyoxal with NH4+ in water at neutral pH, Phys. Chem. Chem.
669 Phys., doi:10.1039/C5CP03113C, 2015.

670 Monge, M. E., Rosenørn, T., Favez, O., Müller, M., Adler, G., Riziq, A. A., Rudich, Y.,
671 Herrmann, H., George, C. and D'Anna, B.: Alternative pathway for atmospheric particles
672 growth, Proc. Natl. Acad. Sci., 109(18), 6840–6844, doi:10.1073/pnas.1120593109, 2012.

673 Monks, P. S.: Gas-phase radical chemistry in the troposphere, Chem. Soc. Rev., 34(5), 376–395,
674 doi:10.1039/B307982C, 2005.

675 Nozière, B., Dziedzic, P. and Córdova, A.: Products and Kinetics of the Liquid-Phase Reaction
676 of Glyoxal Catalyzed by Ammonium Ions (NH4+), J. Phys. Chem. A, 113(1), 231–237,
677 doi:10.1021/jp8078293, 2009.

678 Rossignol, S., Aregahegn, K. Z., Tinel, L., Fine, L., Nozière, B. and George, C.: Glyoxal induced
679 atmospheric photosensitized chemistry leading to organic aerosol growth, Environ. Sci.
680 Technol., 48(6), 3218–3227, doi:10.1021/es405581g, 2014.

681 Sander, S. P., Abbatt, J., Barker, J. R., Burkholder, J. B., Friedl, R. R., Golden, D. M., Huie, R.
682 E., Kolb, C. E., Kurylo, M. J., Moortgat, G. K., Orkin, V. L. and Wine, P. H.: Chemical Kinetics
683 and Photochemical Data for Use in Atmospheric Studies, Evaluation No. 17, JPL Publ. 10-6, Jet
684 Propulsion Laboratory, Pasadena [online] Available from: http://jpldataeval.jpl.nasa.gov, 2011.

685 Sareen, N., Schwier, A. N., Shapiro, E. L., Mitroo, D. and McNeill, V. F.: Secondary organic
686 material formed by methylglyoxal in aqueous aerosol mimics, Atmos Chem Phys, 10(3), 997–
687 1016, doi:10.5194/acp-10-997-2010, 2010.

688 Schwarzenbach, R. P., Gschwend, P. M. and Imboden, D. M.: Environmental Organic
689 Chemistry, 2 edition., Wiley-Interscience, New York., 2002.

690 Shapiro, E. L., Szprengiel, J., Sareen, N., Jen, C. N., Giordano, M. R. and McNeill, V. F.: Light-
691 absorbing secondary organic material formed by glyoxal in aqueous aerosol mimics, Atmos
692 Chem Phys, 9(7), 2289–2300, doi:10.5194/acp-9-2289-2009, 2009.

Sheehy, P. M., Volkamer, R., Molina, L. T. and Molina, M. J.: Oxidative capacity of the Mexico City atmosphere – Part 2: A ROx radical cycling perspective, Atmos Chem Phys, 10(14), 6993–7008, doi:10.5194/acp-10-6993-2010, 2010.

Stemmler, K., Ammann, M., Donders, C., Kleffmann, J. and George, C.: Photosensitized reduction of nitrogen dioxide on humic acid as a source of nitrous acid, Nature, 440(7081), 195–198, doi:10.1038/nature04603, 2006.

Stemmler, K., Ammann, M., Elshorbany, Y., Kleffmann, J., Ndour, M., D'Anna, B., George, C. and Bohn, B.: Light induced conversion of nitrogen dioxide into nitrous acid on submicron humic acid aerosol, Atmospheric Chem. Phys. Discuss., 7, 4035–4064, 2007.

Sumner, A. J., Woo, J. L. and McNeill, V. F.: Model Analysis of Secondary Organic Aerosol Formation by Glyoxal in Laboratory Studies: The Case for Photoenhanced Chemistry, Environ. Sci. Technol., 48(20), 11919–11925, doi:10.1021/es502020j, 2014.

Teich, M., van Pinxteren, D., Kecorius, S., Wang, Z. and Herrmann, H.: First Quantification of Imidazoles in Ambient Aerosol Particles: Potential Photosensitizers, Brown Carbon Constituents, and Hazardous Components, Environ. Sci. Technol., 50(3), 1166–1173, doi:10.1021/acs.est.5b05474, 2016.

Thalman, R. and Volkamer, R.: Inherent calibration of a blue LED-CE-DOAS instrument to measure iodine oxide, glyoxal, methyl glyoxal, nitrogen dioxide, water vapour and aerosol extinction in open cavity mode, Atmos Meas Tech, 3(6), 1797–1814, doi:10.5194/amt-3-1797-2010, 2010.

Thalman, R. and Volkamer, R.: Temperature dependent absorption cross-sections of O2–O2 collision pairs between 340 and 630 nm and at atmospherically relevant pressure, Phys. Chem. Chem. Phys., 15(37), 15371–15381, doi:10.1039/C3CP50968K, 2013.

Thalman, R., Zarzana, K. J., Tolbert, M. A. and Volkamer, R.: Rayleigh scattering cross-section measurements of nitrogen, argon, oxygen and air, J. Quant. Spectrosc. Radiat. Transf., 147, 171–177, doi:10.1016/j.jqsrt.2014.05.030, 2014.

Thalman, R., Baeza-Romero, M. T., Ball, S. M., Borrás, E., Daniels, M. J. S., Goodall, I. C. A., Henry, S. B., Karl, T., Keutsch, F. N., Kim, S., Mak, J., Monks, P. S., Muñoz, A., Orlando, J., Peppe, S., Rickard, A. R., Ródenas, M., Sánchez, P., Seco, R., Su, L., Tyndall, G., Vázquez, M., Vera, T., Waxman, E. and Volkamer, R.: Instrument intercomparison of glyoxal, methyl glyoxal and NO2 under simulated atmospheric conditions, Atmos Meas Tech, 8(4), 1835–1862, doi:10.5194/amt-8-1835-2015, 2015.

Trainic, M., Abo Riziq, A., Lavi, A., Flores, J. M. and Rudich, Y.: The optical, physical and chemical properties of the products of glyoxal uptake on ammonium sulfate seed aerosols, Atmos Chem Phys, 11(18), 9697–9707, doi:10.5194/acp-11-9697-2011, 2011.

Vandaele, A. C., Hermans, C., Fally, S., Carleer, M., Colin, R., Mérienne, M.-F., Jenouvrier, A. and Coquart, B.: High-resolution Fourier transform measurement of the NO2 visible and near-

infrared absorption cross sections: Temperature and pressure effects, J. Geophys. Res. Atmospheres, 107(D18), 4348, doi:10.1029/2001JD000971, 2002.

Volkamer, R., San Martini, F., Molina, L. T., Salcedo, D., Jimenez, J. L. and Molina, M. J.: A missing sink for gas-phase glyoxal in Mexico City: Formation of secondary organic aerosol, Geophys. Res. Lett., 34(19), L19807, doi:10.1029/2007GL030752, 2007.

Volkamer, R., Sheehy, P., Molina, L. T. and Molina, M. J.: Oxidative capacity of the Mexico City atmosphere – Part 1: A radical source perspective, Atmos Chem Phys, 10(14), 6969–6991, doi:10.5194/acp-10-6969-2010, 2010.

Washenfelder, R. A., Langford, A. O., Fuchs, H. and Brown, S. S.: Measurement of glyoxal using an incoherent broadband cavity enhanced absorption spectrometer, Atmos Chem Phys, 8(24), 7779–7793, doi:10.5194/acp-8-7779-2008, 2008.

Weller, C., Horn, S. and Herrmann, H.: Effects of Fe(III)-concentration, speciation, excitation-wavelength and light intensity on the quantum yield of iron(III)-oxalato complex photolysis, J. Photochem. Photobiol. Chem., 255, 41–49, doi:10.1016/j.jphotochem.2013.01.014, 2013a.

Weller, C., Horn, S. and Herrmann, H.: Photolysis of Fe(III) carboxylato complexes: Fe(II) quantum yields and reaction mechanisms, J. Photochem. Photobiol. Chem., 268, 24–36, doi:10.1016/j.jphotochem.2013.06.022, 2013b.

Yi, J., Bahrini, C., Schoemaecker, C., Fittschen, C. and Choi, W.: Photocatalytic Decomposition of H2O2 on Different TiO2 Surfaces Along with the Concurrent Generation of HO2 Radicals Monitored Using Cavity Ring Down Spectroscopy, J. Phys. Chem. C, 116(18), 10090–10097, doi:10.1021/jp301405e, 2012.

Yu, G., Bayer, A. R., Galloway, M. M., Korshavn, K. J., Fry, C. G. and Keutsch, F. N.: Glyoxal in Aqueous Ammonium Sulfate Solutions: Products, Kinetics and Hydration Effects, Environ. Sci. Technol., 45(15), 6336–6342, doi:10.1021/es200989n, 2011.

Zardini, A. A., Sjogren, S., Marcolli, C., Krieger, U. K., Gysel, M., Weingartner, E., Baltensperger, U. and Peter, T.: A combined particle trap/HTDMA hygroscopicity study of mixed inorganic/organic aerosol particles, Atmos Chem Phys, 8(18), 5589–5601, doi:10.5194/acp-8-5589-2008, 2008.

Zellner, R., Exner, M. and Herrmann, H.: Absolute OH quantum yields in the laser photolysis of nitrate, nitrite and dissolved H2O2 at 308 and 351 nm in the temperature range 278-353 K, J. Atmospheric Chem., 10, 411–425, 1990.

Zhao, R., Lee, A. K. Y., Soong, R., Simpson, A. J. and Abbatt, J. P. D.: Formation of aqueous-phase α-hydroxyhydroperoxides (α-HHP): potential atmospheric impacts, Atmos Chem Phys, 13(12), 5857–5872, doi:10.5194/acp-13-5857-2013, 2013.

766

767 **Figures**
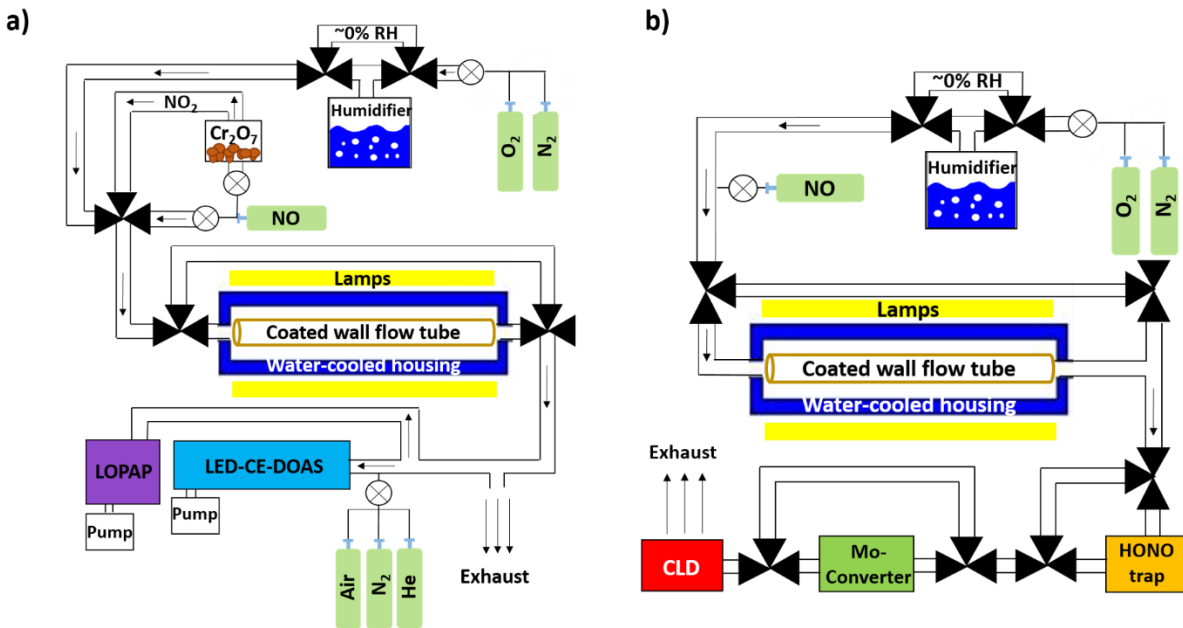
768

769 Figure 1. Sketch of the photochemical flow tube reactor setups at PSI for a) Setup 1 in 2013

770 measuring NO_2 generation and b) for Setup 2 in 2014 measuring NO loss.

771
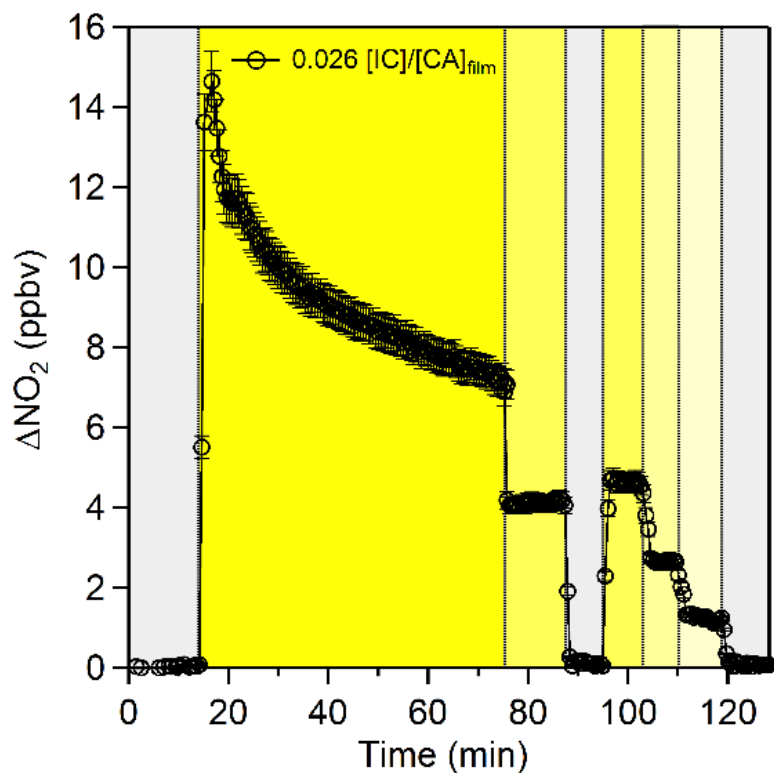
772

773

774   Figure 2. NO_2 profile for a 0.025M IC bulk solution, whose concentration increases to ~0.2 M of

775   IC in the film due to the citric acid hygroscopic properties. The gray shaded areas indicate

776   periods where NO was exposed in the dark. The yellow shaded areas indicates the period of

777   irradiation; the decrease in the intensity of yellow represents the decrease in irradiance (2.26 x

778   10^{16}, 1.47 x 10^{16}, 1.14 x 10^{16}, and 3.94 x 10^{15} photons cm^{-2} s^{-1}, for seven, five, three and one

779   lamp, respectively). This timeseries clearly indicates the light dependence production of HO_2

780   radicals from the photosensitization of IC in a CA film.

781

782

783
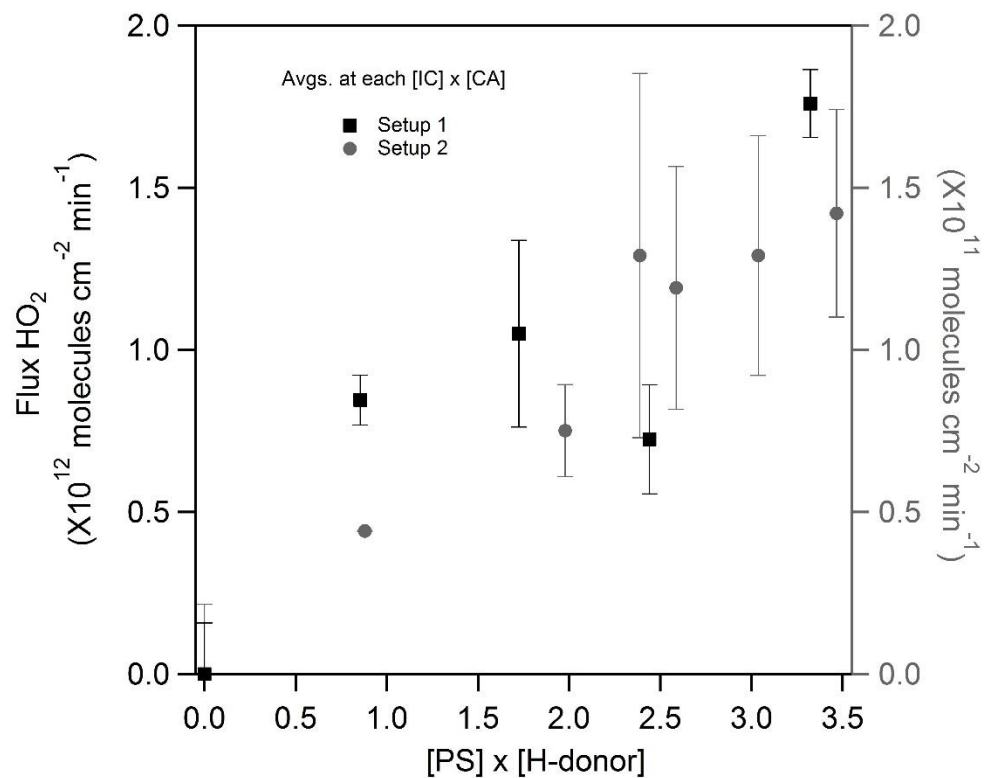
Figure 3. A linear correlation of HO_2 as a function of IC concentration. The left y-axis

represents the values for Setup 1, while the right y-axis represents the values for Setup 2, (an

order of magnitude difference for both scales). The Setup 2 data falls between a factor of 2 and 3

from Setup 1 after accounting for differences between Setup 1 and 2, see Sect. 3.1.1.

788
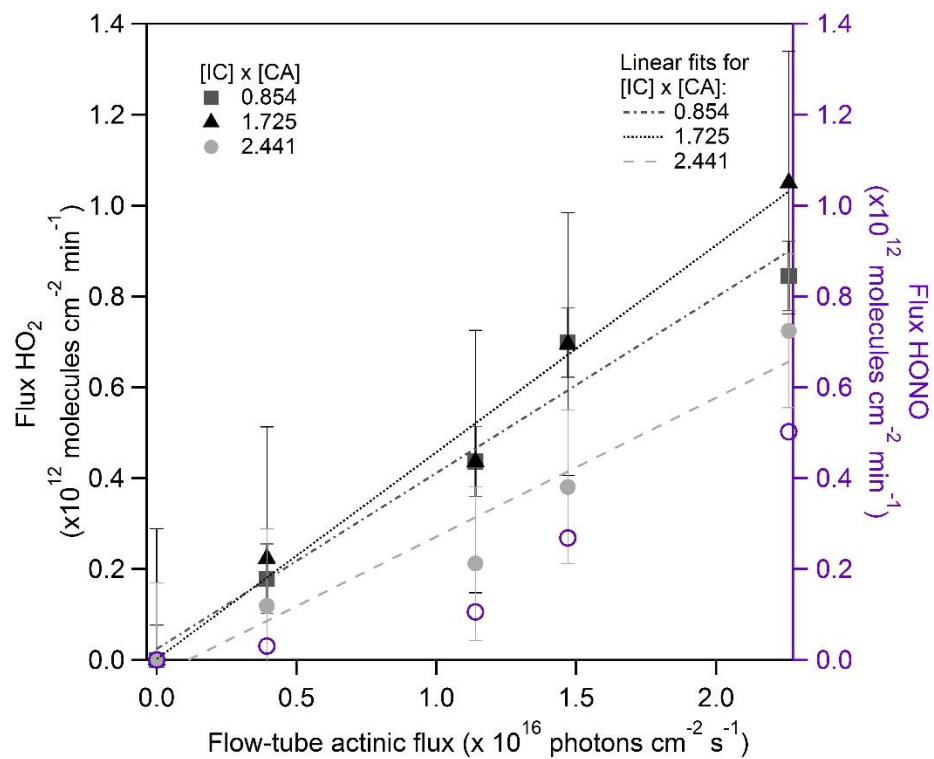
789

790

791   Figure 4. HO_2 fluxes <u>in</u> (molecules cm^{-2} min^{-1}) as a function of actinic flux for a 300-420 nm

792   range <u>(solid symbols)</u>. The data is plotted as a concentration product of [IC] x [CA] (shown in

793   the legend) which shows the photochemical reaction between IC and CA in H_2O matrix and

794   gaseous NO. HONO for 2.441 ([IC] x [CA]) is plotted on the right axis <u>(open circles)</u>, showing

795   a ratio of $HONO:NO_2 < 1$, which suggests OH as a secondary product.

796

The y-axis is labeled "Flux HO_2 ($\times 10^{11}$ molecules cm^{-2} min^{-1})" and the x-axis is labeled "Relative humidity (%)".
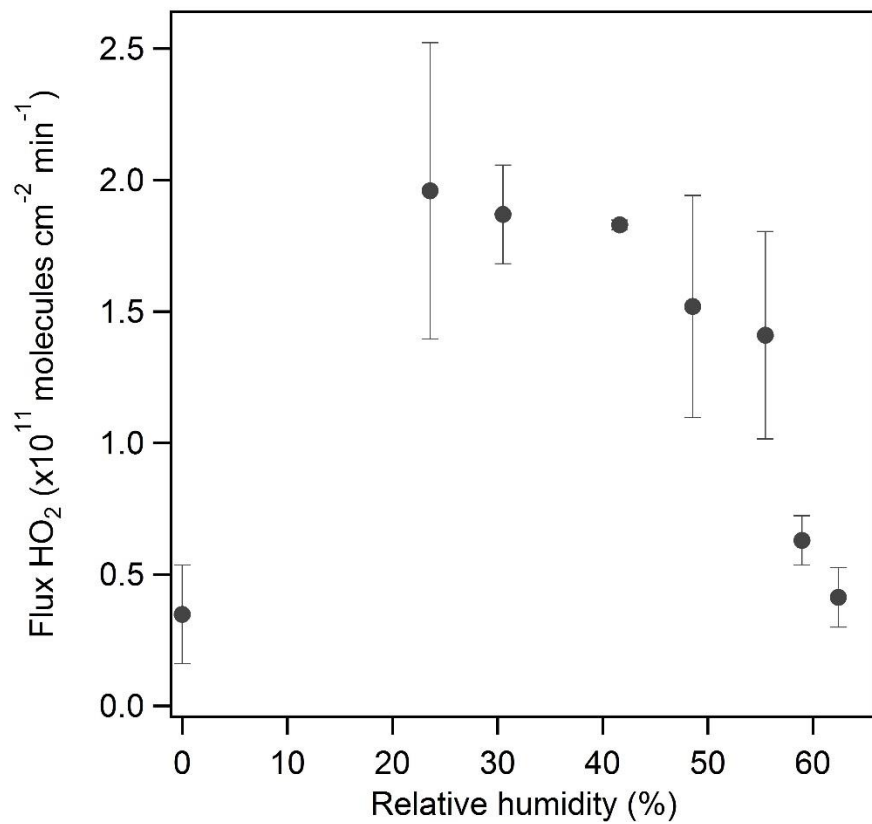
797

798

799   Figure 5. The NO loss normalized to the film surface area as a function of relative humidity.

800
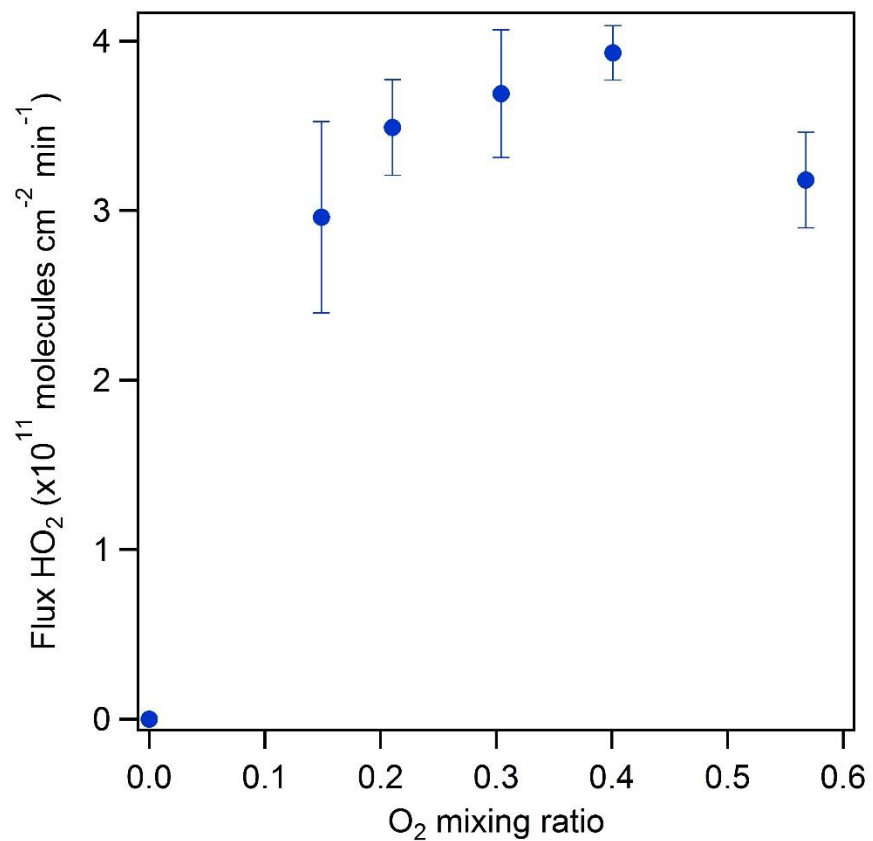
Figure 6. Measured loss of NO above a film composed of IC and CA normalized of the film surface area as a function of the O_2 mixing ratio.

806
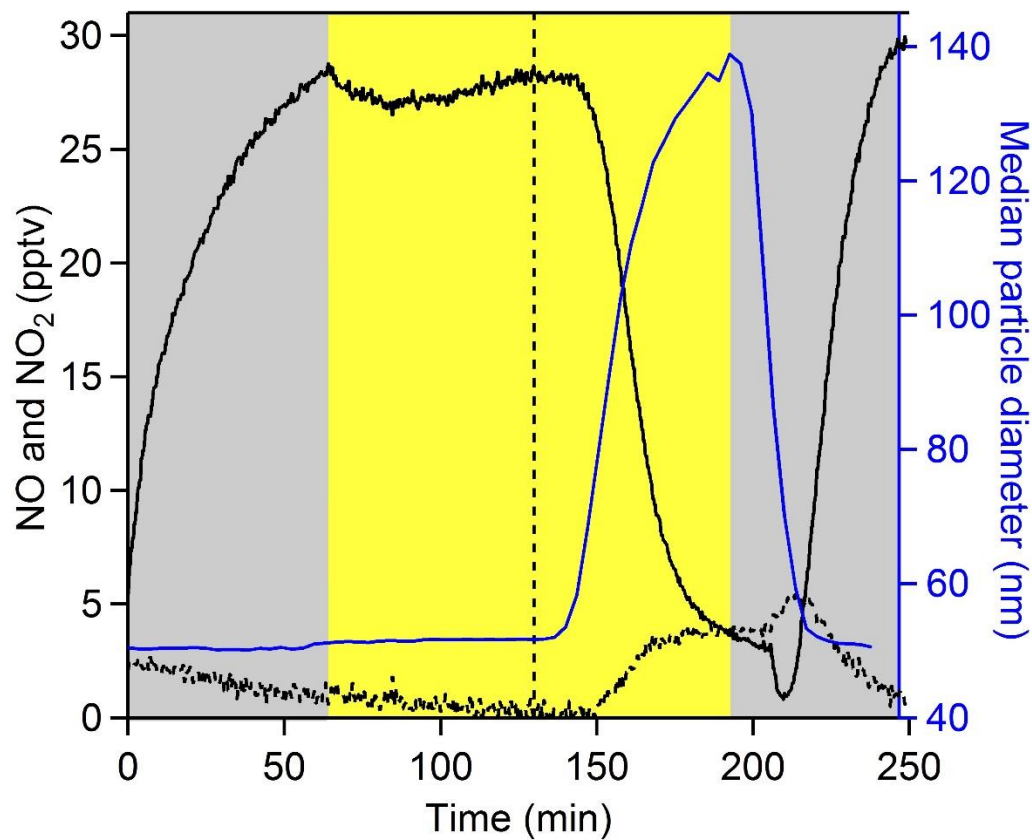
807

808   Figure 7. Aerosol flow tube experiments show rapid conversion of NO (solid black line) into

809   NO$_2$ (dashed black line)   only after the time when limonene (gaseous H-donor) is added into the

810   flowtube (vertical dashed line). The gray shaded areas represent experiment in the dark, and the

811   yellow shaded area represents the experiment under light exposure. The blue line represents the

812   growth of aerosols, right axis.

813
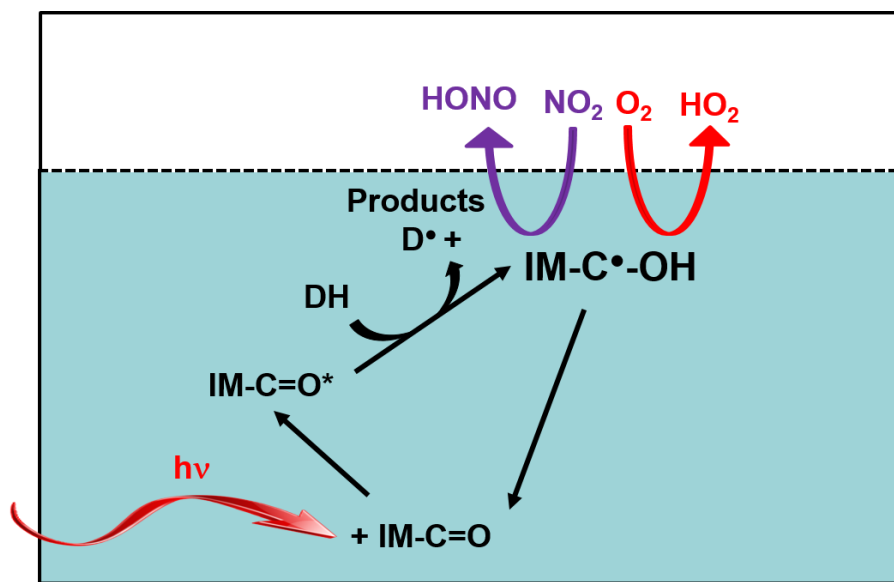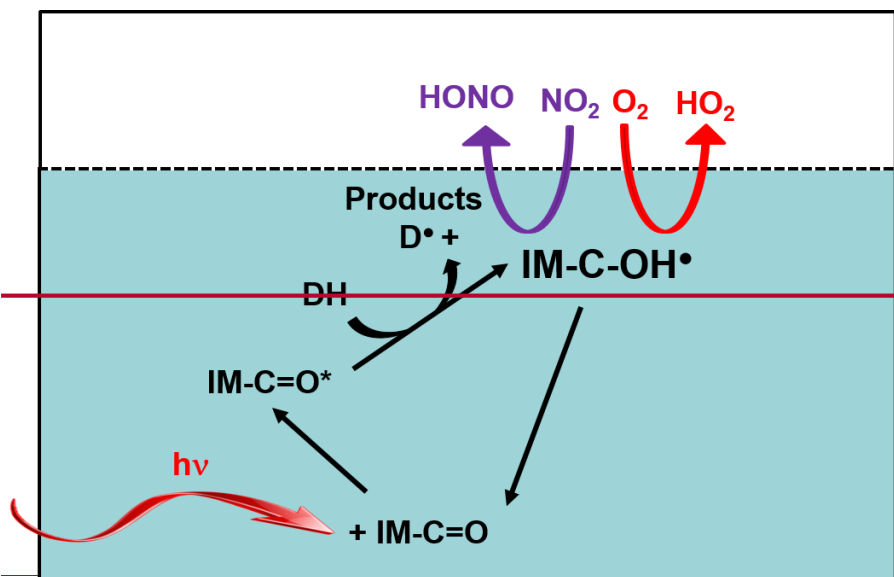
Figure 8. Proposed mechanism, modified and expanded to photosensitization of IC based on Canonica et al. (1995), George et al. (2005) and Aregahegn et al. (2013). The reaction in the white square represents the gas-phase, and the blue square represents the aqueous phase. DH is an H-donor (e.g. CA, another IC, H2O+CA matrix to be determined from flash photolysis).

33

Heterogeneous photochemistry of imidazole-2-carboxaldehyde: HO$_2$ radical formation and aerosol growth

L. González Palacios et al.

NO$_2$ actinometry

The actinic flux (photons cm^{-2} sec^{-1}) was measured with one, three, five and all seven lamps of the photo reactor turned on using NO$_2$ actinometry (method A), and independent measurements of the photon actinic flux (method B). With method A, NO$_2$ in a N$_2$/O$_2$ gas mixture was added to the flow-tube under two different configurations: a) a bare glass flow-tube, and b) a blank coated flow-tube consisting of CA only, in the absence of IC. The NO$_2$ gas was produced from the oxidation of a gas flow of NO through a chromate salt reservoir, shown in Fig. 1A. In configuration a), the concentration of NO$_2$ was about 8 ppbv and in configuration b) it was about 40 ppbv. NO$_2$ actinometry is based on the following reaction:

$$NO_2 + h\nu \rightarrow NO + O(^3P) \qquad\qquad (\text{R1})$$

The photolysis constant, J, in our case was treated as first-order rate constant, which quantifies the rate of photolysis of NO$_2$, J_{NO2}, in terms of a relative concentration change over time. The decrease in NO$_2$ was measured by the LED-CE-DOAS (Setup 1) and by the chemiluminescence (Setup 2); the NO$_2$ signal was allowed to stabilize, and lights were turned on sequentially. J_{NO2} was calculated using the measurements and the following equation:

$$J_{NO2} = \frac{d\,ln[NO_2]}{dt}, \qquad\qquad -ln\left(\frac{[NO_2]_t}{[NO_2]_0}\right) = J_{NO2} \times t \qquad\qquad (\text{S1})$$

With all seven lamps turned on, the J_{NO2} was about 2×10^{-2} s^{-1} (Setup 1) and 1×10^{-2} s^{-1} (Setup 2). This is about 2-3 times the ambient J at mid-latitudes under summer noon-time conditions. The J_{NO2} for configurations a) and b) are compared in the Fig. S2, and agreed within 8 % at 7 lamps and this variability increases as the number of lamps (irradiation) decrease, up to a factor of 2 as a maximum.

The *J*-values of NO$_2$ were calculated using independent measurements of the photon actinic flux of the UV lamps, which had been determined by B. Bohn at Forschungzentrum Jülich (Germany) with a LICOR 1800 hemispherical, cosine corrected spectro-radiometer (method B). The following equation was used to calculate the first order photolysis rate, *J*-value:

$$J - value = \int_{300}^{420} F_{FT}(\lambda)\, \sigma(\lambda)\Phi(\lambda)d\lambda \qquad (S2)$$

where $F_{FT}(\lambda)$ is the actinic flux measured in our flow-tube system, $\sigma(\lambda)$ is the NO$_2$ cross section at 294 K in cm^2 molecule^{-1} (Vandaele et al., 2002), and $\Phi(\lambda)$ is the quantum yield data used from Sander et al., 2011. The *J*-values for NO$_2$ for methods A and B are compared in Fig. S2, and agree within a factor of 2 (higher *J*$_{NO2}$ for method A). The photon actinic flux shown in the Fig. S3 has been adjusted by this factor, and is compared with a typical solar spectral irradiance at the Earth surface (solar zenith of 48°, The American Society for Testing and Materials, ASTM).

Equation S1 shows the relationship between the loss of NO$_2$, the derived pseudo-first order *J*$_{NO2}$ and the uptake coefficient (γ) for a heterogeneous reaction in a cylindrical flow-tube:

$$\frac{d[NO_2]}{dt} = -JNO_2[NO_2] \qquad\qquad JNO_2 = \frac{\gamma <c> [\frac{S}{V}]}{4} \qquad (S3)$$

where $<c>$ is the NO$_2$ mean molecular speed, $(8RT/\pi M)^{1/2}$, and $[\frac{S}{V}]$ is the surface are of the film per gas volume ratio in our flow-tube system. These calculations are represented in Fig. S4.

Figure Captions

Figure S1: NO_2 j-values in s^{-1} from the bare glass and citric acid blank coated flow-tubes in Setup 1.

Figure S2: Determination of the NO concentration in the 2014 PSI flow-tube system. The lifetime of HO_2 is short enough at 500 ppbv with respect to its reaction with NO. This ensures a 1 NO:1 HO_2 molecular reaction in our experimental conditions. An IM/AC ratio of 0.088 was fixed for this specific experiment.

Figure S3: Solid line: the cross-section of IC in H_2O; the UV-VIS absorption of IC was measured by Kampf et al., 2010 and interpolated to more recent molar extinction measurements by Barbara Nozière at IRCELyon (right scale in cm^2). Shaded gray: calculated wavelength dependent photolysis frequencies of imidazole-2-carboxaldehyde, j-values, based on the calculated quantum yield in our flow tube. Dotted line: actinic flux of the UV-light source in our flow-tube system from 300-420 nm range, the total flux is 2.26×10^{16} photons cm^{-2} s^{-1}. Dashed line: a solar actinic flux spectrum for a solar zenith angle of 48°, 37° tilt towards the sun and clear skies ($\sim 2 \times 10^{16}$ photons cm^{-2} s^- between 300-420 nm) obtained from the standard spectrum of the American Society for Testing and Materials (ASTM).

Figure S4: Film thickness dependence represented by NO loss. The IC:CA ratio was kept constant to show the classic behavior of reactions governed by reaction and diffusion. At low thicknesses, P_{HO2} increases linearly and saturates at thicknesses >2 µm. This shows that the observed HO_2 is produced from the top few micrometers of the films under study.

Figure S5: The photosensitized uptake coefficient of NO_2 (blue diamonds, right axis); this graph shows the inefficiency of NO_2 to compete with O_2 at atmospheric mixing ratios. The open red

circles represent the CA blank measurements, the closed red circles represent a 1.725 [IC] ×

[CA] film measurements during NO$_2$ actinometry experiments (left axis).

Figure S6: NO to NO$_2$ conversion from similar CWFT experiments performed in a different

photosensitizer, 4-BBA. The top figure shows that NO does react with HO$_2$ to produce NO$_2$ in

the presence of 4-BBA and adipic acid (AA), as the organic aqueous base. The bottom figure

shows no conversion in a clean tube.
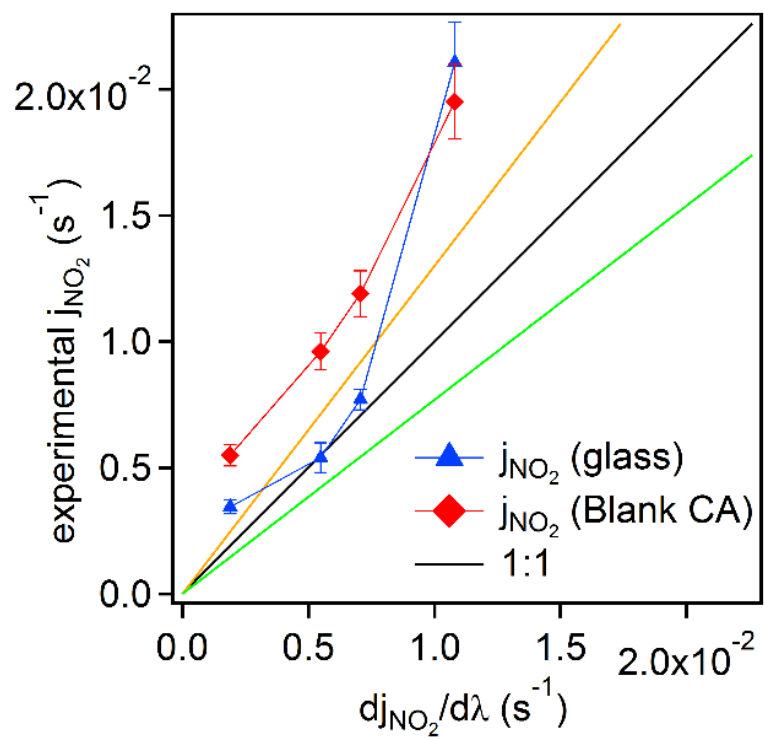
Figure S1
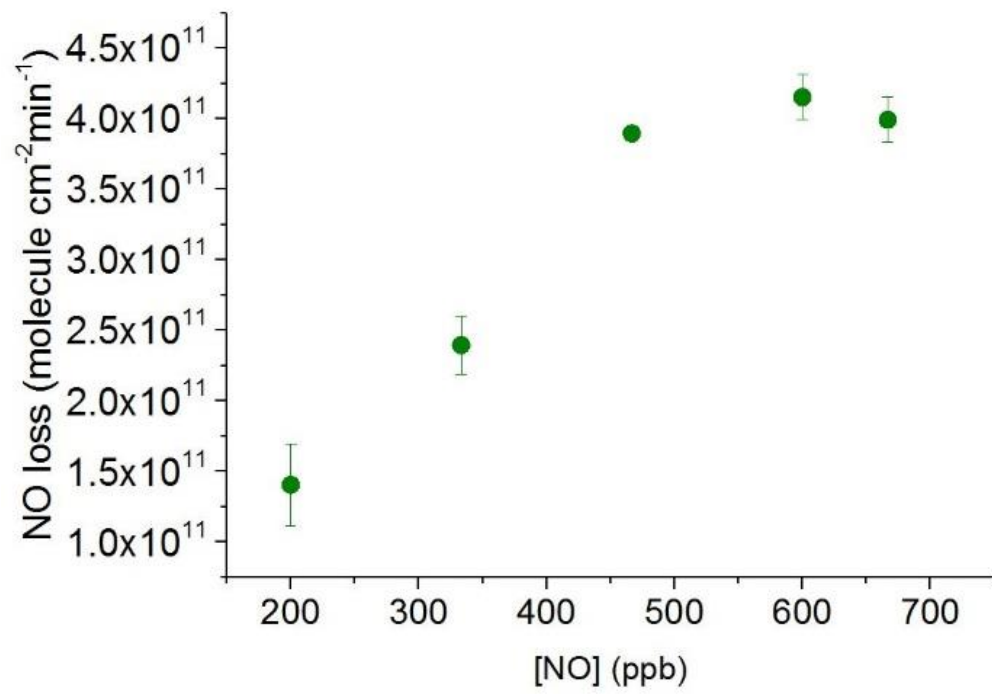
Figure S2
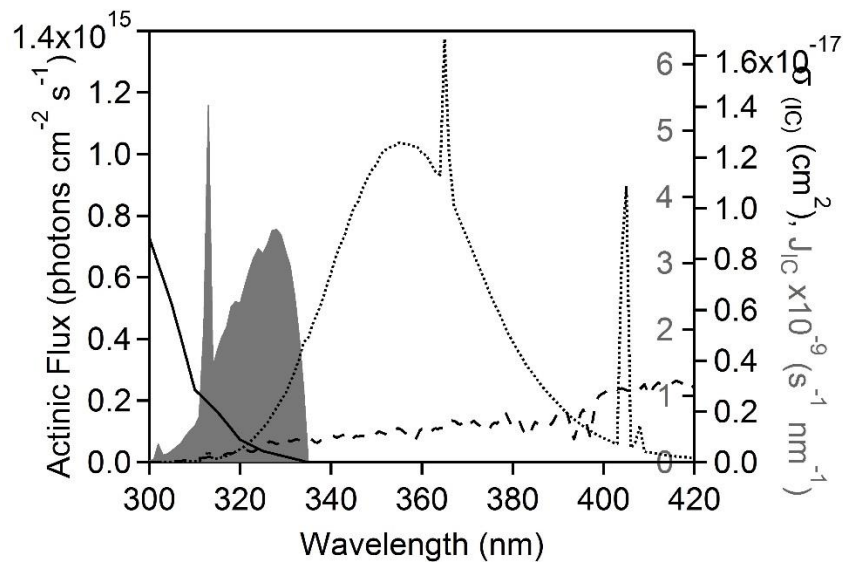
Figure S3
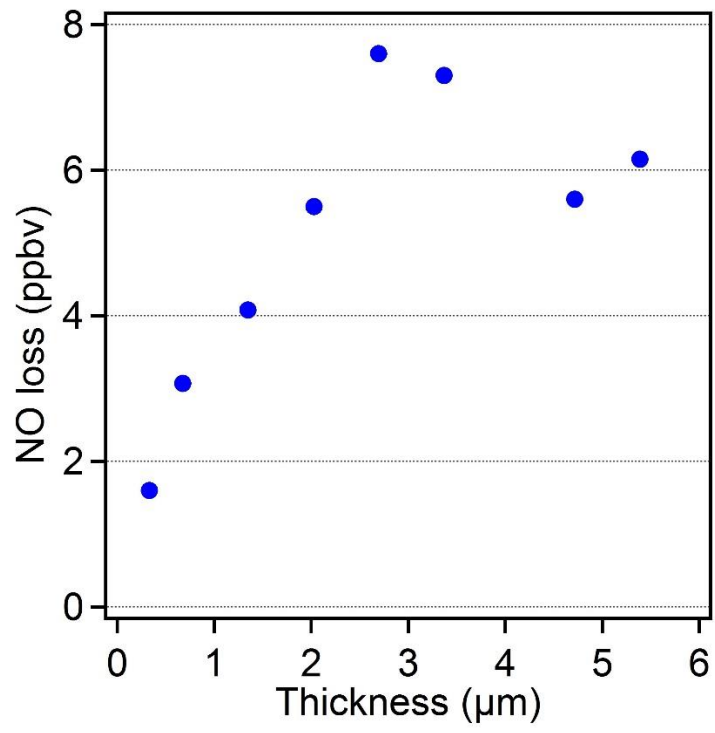
Figure S4

Figure S5

Figure S6